AWARD NUMBER: W81XWH-15-1-0460

TITLE: Protein Dependent Activation of the Unfolded Protein Response (UPR) Enables Prostate Cancer Development and a Druggable Target for Advance Prostate Cancer Therapy

PRINCIPAL INVESTIGATOR: Dr. Hao N. Nguyen, MD

CONTRACTING ORGANIZATION: University of California, San Francisco
San Francisco, CA 94103

REPORT DATE: October 2016

TYPE OF REPORT: ANNUAL

PREPARED FOR: U.S. Army Medical Research and Materiel Command
Fort Detrick, Maryland 21702-5012

REPORT DOCUMENTATION PAGE

Form Approved
OMB No. 0704-0188

1. REPORT DATE	2. REPORT TYPE	3. DATES COVERED
October 2016	ANNUAL	30 Sep 2015 - 29 Sep 2016

4. TITLE AND SUBTITLE

Protein Dependent Activation of the Unfolded Protein Response (UPR) Enables Prostate Cancer Development and a Druggable Target for Advance Prostate Cancer Therapy

5a. CONTRACT NUMBER

5b. GRANT NUMBER
W81XWH-15-1-0460

5c. PROGRAM ELEMENT NUMBER
–

6. AUTHOR(S)
Dr. Hao G. Nguyen, MD.

E-Mail: hao.nguyen@ucsf.edu

5d. PROJECT NUMBER
–

5e. TASK NUMBER
–

5f. WORK UNIT NUMBER
–

7. PERFORMING ORGANIZATION NAME(S) AND ADDRESS(ES)
University of California, San Francisco
1855 Folsom Street, MCB, Suite # 425, Box # 0897
San Francisco, CA-94143-0897

8. PERFORMING ORGANIZATION REPORT NUMBER
-

9. SPONSORING / MONITORING AGENCY NAME(S) AND ADDRESS(ES)

U.S. Army Medical Research and Materiel Command
Fort Detrick, Maryland 21702-5012

10. SPONSOR/MONITOR'S ACRONYM(S)
–

11. SPONSOR/MONITOR'S REPORT NUMBER(S)
–

12. DISTRIBUTION / AVAILABILITY STATEMENT

Approved for Public Release; Distribution Unlimited

13. SUPPLEMENTARY NOTES

14. ABSTRACT

The acquisition of oncogenic lesions stimulates biosynthetically and bioenergetically demanding cellular processes such as protein synthesis to drive cancer cell growth and proliferation. The hijacking of these key processes by oncogenic pathways triggers cellular stress that requires an adaptive or evasive response in order for cancer cells to survive and continue proliferating. The UPR is a cellular homeostatic program engaged when an excess of unfolded/misfolded proteins accumulate within the lumen of the endoplasmic reticulum. It is carried out by three major signaling arms: PERK, IRE1, and ATF6. However, whether and how each of these distinct signaling arms of the UPR is specifically activated by deregulated protein synthesis upon oncogenic insult is poorly understood.

We showed that prostate cancer initiation and maintenance, following combined loss of the PTEN tumor suppressor and overexpression of the Myc oncogene, rely on protein synthesis-dependent activation of the UPR to facilitate tumor cell survival. Specifically, we have employed a novel genetic mouse model coupling PTEN loss with MYC overexpression in the prostate and we observe that overexpression of Myc in the prostate synergizes with PTEN loss to dramatically stimulate the PERK and IRE1 signaling arms of the UPR pathway, which correlates with enhanced PIN formation and invasive carcinoma. To dissect the mechanism by which these oncogenic lesions promote UPR signaling, we employed human prostate epithelial cells overexpress MYC, harbor an shRNA targeting PTEN, or the combined overexpression of MYC and shRNA of PTEN. We demonstrate the activation of UPR arms PERK and IRE1 upon oncogenic transformation by Myc overexpression and loss of PTEN. Interestingly, blocking the cytoprotective UPR using PERK or IRE1 inhibitors resulted in a significant increase in cell death and decreased clonogenic potential in cells harboring both oncogenic lesions (MYC/PTEN), but not in normal cells.

Furthermore, we are currently evaluating UPR inhibition in a preclinical trial utilizing our *in vivo* PTEN loss model with or without MYC overexpression using several models of patient derived xenograft (PDX) model of high risk prostate cancer. In addition, we are utilizing gene expression analysis to understand the mechanistic connection between protein synthesis and the specific arms of the UPR. Taken together, our results suggest a critical role of the UPR in ensuring prostate cancer cell progression and serve as a promising opportunity for therapeutically targeting this cancer-specific vulnerability to stress adaptation in order to elicit synthetic lethality.

Impact statement:

Delineate the mechanisms underlying stress response pathways, in particular the unfolded protein response (UPR), in novel mouse models (MYC hyperactivation/PTEN knock down) and human prostate cancer, and investigate novel therapies to target stress response pathways.

15. SUBJECT TERMS

Unfolded protein response, therapeutic target for lethal prostate cancer, patient derived Xenografts, translational regulation, PTEN, MYC

16. SECURITY CLASSIFICATION OF:			**17. LIMITATION OF ABSTRACT**	**18. NUMBER OF PAGES**	**19a. NAME OF RESPONSIBLE PERSON**
a. REPORT	**b. ABSTRACT**	**c. THIS PAGE**			USAMRMC
U	U	U	UU	26	**19b. TELEPHONE NUMBER** *(include area code)*

Table of Contents

Page

INTRODUCTION:

The acquisition of oncogenic lesions stimulates biosynthetically and bioenergetically demanding cellular processes such as protein synthesis to drive cancer cell growth and proliferation. The hijacking of these key processes by oncogenic pathways triggers cellular stress that requires an adaptive or evasive response in order for cancer cells to survive and continue proliferating. We have previously demonstrated that deregulated protein synthesis, which is induced by oncogenic signaling pathways such as Myc and PI3K that are commonly activated in prostate cancer, activates one of the key cytoprotective stress response pathways, known as the unfolded protein response (UPR). The UPR is a cellular homeostatic program engaged when an excess of unfolded/misfolded proteins accumulate within the lumen of the endoplasmic reticulum. It is carried out by three major signaling arms: PERK, IRE1, and ATF6. However, whether and how each of these distinct signaling arms of the UPR is specifically activated by deregulated protein synthesis upon oncogenic insult is poorly understood.

An outstanding question is how the UPR pathways are regulated and maintained in prostate cancer initiation and maintenance. In addition, our previous work has indicated that the other adverse environmental conditions including chemotherapy, androgen deprivation, radiation, the UPR is activated to ensure cell survival[6]. The UPR is both pro-survival and pro-death. Why does it promote survival cancer cells and pro-death in other settings? Can UPR-targeted therapeutics be designed to separate pro-survival and apoptotic responses? Strikingly, our preliminary data demonstrate that both MYC and PTEN loss cooperate to activate the UPR and are critical in tumor cell survival and oncogenic transformation. These findings lay the foundation for this proposal, which seeks to open a new portal into our understanding of mechanisms that maintain the adaptation of cancer cells to stress and develops a novel therapeutic regimen to target this vulnerability of transformed cells.

KEYWORDS:

Prostate cancer, unfolded protein response, oncogenic stress, PTEN, MYC, patient derived xenografts, novel therapeutic approach for metastatic prostate cancer.

ACCOMPLISHMENTS:

What were the major goals of the project?

- Approved SOW

Major Task 1: To assess the role protein synthesis-dependent control of the unfolded protein response in prostate cancer development and maintenance in vivo.
Subtask 1: To assess the role of protein synthesis-dependent control of the unfolded protein response in prostate cancer development in vivo. (12 months) Cell lines used: mouse prostate epithelial isolated from PTENloxlox/Myc++ invivo model Accomplished 80%
Subtask 2: Expand PB-Cre;MYCtg;PTENloxP/loxP mouse colonies (4 months) Perform preclinical trial using IRE-1 inhibitor in 4 week cycles and evaluate for tumor progression starting with 1 month old mice. (3 months) Accomplished: 100%
Subtask 3: Perform preclinical trial using IRE-1 inhibitor in 4 week cycles and evaluate for tumor regression. Subtask 4: To analyze differences in protein synthesis in vivo, we will measure the amount of

35S-methionine incorporation of cultured PB-Cre; MYCtg;PTENloxP/loxP prostate cancer cells. Analysis of 35Smethionine incorporation in murine prostate cancer after treatment with PERK or IRE inhibitor. (2 months) Accomplished 100%		
Subtask 5: Prostates will be harvested for immunohistochemical evaluation of global protein synthesis components downstream of PTEN loss/mTOR (for example, phospho-4EBP1, phospho-rpS6 and phospho-eIF4E) as well as for proliferation and cell survival (Ki-67 and TUNEL analysis, respectively). (1 month) Accomplished 100%		
Milestone(s) Achieved: *Determine the role of UPR in prostate cancer initiation and maintenance, obtain preclinical data with UPR inhibitors on inhibition of tumor growth in the early stage setting.*		
Milestone(s) Achieved: Determine the therapeutic potential of inhibiting protein-dependent control of the UPR in early stage and late stage metastatic prostate cancer with validation of human samples, hence providing data for phase1/2 clinical trial. publication of 1-2 peer reviewed papers	36-48 Months	Dr. Nguyen

- **What was accomplished under these goals?**

To assess the role protein synthesis-dependent control of the unfolded protein response in prostate cancer development and maintenance in vivo.

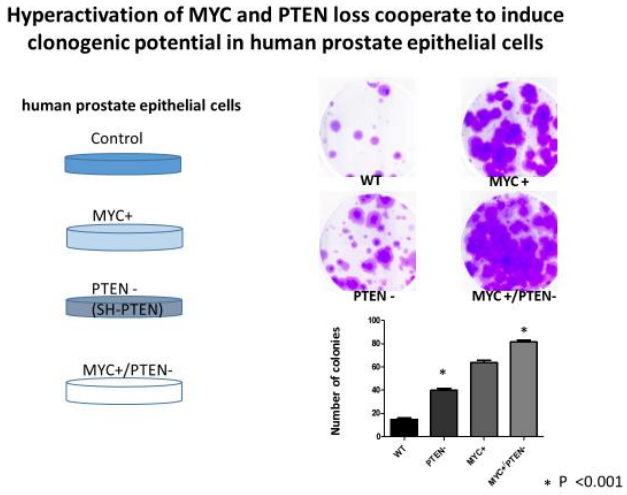

Figure 1. Knock-down of PTEN and overexpression of MYC in human prostate epithelial cells induced transformation.

The most common driver mutations implicated in prostate cancer are MYC overexpression and PTEN loss. The mechanism of prostate cancer tumorigenesis induced by aberrant PI3K-AKT-mTOR signaling is largely mediated through the downstream activation of the kinase mTOR, while MYC overexpression results in activation of multiples pathway to promote cellular progression. How oncogenic stresses or tumor microenvironmental stresses activate the UPR remain poorly understood. Is there a specific translational program that is activated to induce the UPR? In this aim, I seek to define the underlying molecular mechanisms by which a novel regulatory translational program selects for specific mRNAs, conferring sensitivity to activation PERK and IRE-1. I will determine the impact of PTEN/mTOR/4EBP-1-eIF4E on activation of the three major arms of the UPR pathway (ATF6, PERK, and IRE-1) during oncogenic transformation and

evaluate the therapeutic potential of inhibiting eIF4E-dependent control of the UPR. To address this aim, we have generated human prostate epithelia cells (PrEc) with stable expression of MYC and stable knockdown of PTEN using short hairpin targeting PTEN cDNA or the 3' UTR. We also generated the cells with combination of MYC overexpression and PTEN knock down as shown in Figure 1.

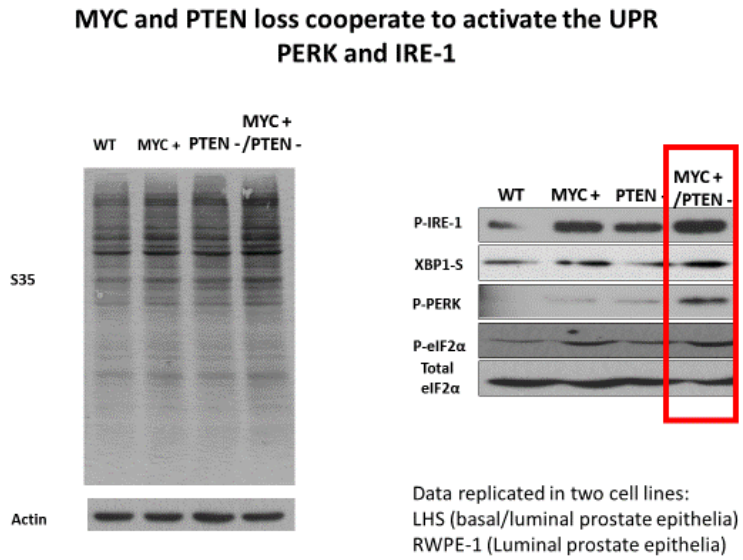

Figure 2a. Left panel showed analysis of 35Smethionine incorporation in human prostate epithelial cells line. Right panel showed activation of UPR pathway using XBP-1s and phosphor PERK and phosphor-eIF2a as markers.

Activation of the URP is associated with increased in global protein synthesis. Experiments are underway to evaluate global protein synthesis incorporation of murine prostate cancer after treatment with PERK or IRE inhibitor.

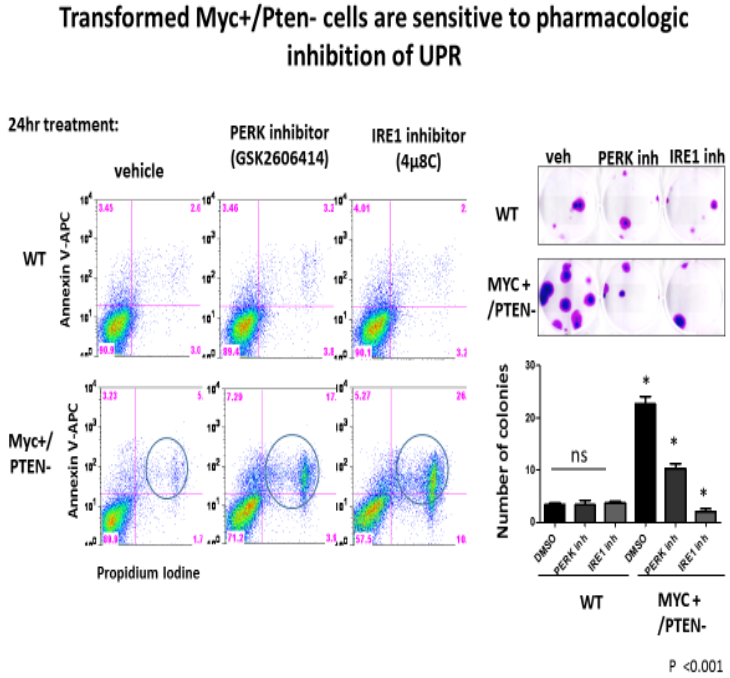

Figure 3. Flow cytometry analysis of apoptosis as measured by Annexin V staining (left panel). Increased in apoptosis were observed only on Myc+/PTEN loss cell but not WT. Right panel showed inhibition of colony formation. Note that only cells with UPR activation (MYC hyperactivation and PTEN loss) were effected.

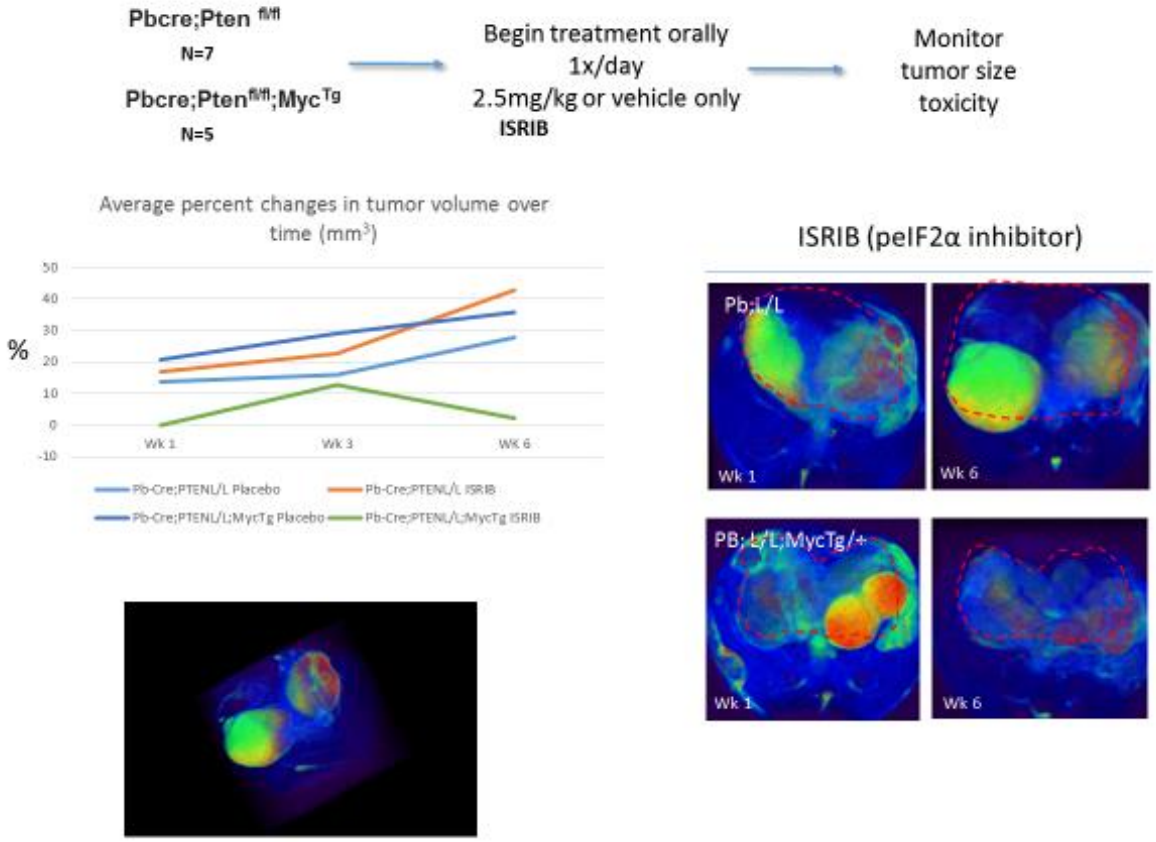

Figure 4. Preclinical trial using ISRIB (inhibitor of Stress Response, phosphor-eIF2a) Left panel. Right panel showed MRI of tumor. Tumor regression were observed only in the PB-Cre; MYCtg;PTENloxP/loxP mice treated with ISRIB.

Starting work on goal for year 2-3 of the grant.

Major Task 3: To define the unfolded protein response (UPR) in promote tumor progression in castrate resistant prostate cancer and in therapy resistant setting. Subsequently to determent if targeting the URP in this setting may improve response and delay disease progression

Establish a new cohort of PDX models to test the therapeutic benefit of inhibiting eIF2a phosphorylation and other UPR arms on the growth of primary human and metastatic prostate cancer samples.

Here we seek a new paradigm to characterize and test novel therapeutics using the most relevant invivo model to recapitulate the diverse and heterogeneity of prostate cancer across risk spectrum. Despite advances in novel drug design and new insights into the genetic landscape advance local-regional and metastatic prostate cancer, most new therapies failed to show survival benefits prior to reaching phase 3 in clinical trials. This translational gap is in-part due to the limitation of current cell-based xenografts models used in preclinical testing and often lead to a substantially different response profile when tested in human. To this end, we aim to create a more predictive and more precise model of prostate cancer using tumors (primary and metastasis) taken directly from patients (also known as Patient-Derived Xenografts or PDXs) and implant directly into an immunodeficient mouse. To accomplish this specific aim, we will obtain patient tumors immediately after devascularization of the prostate during surgery to minimize any further cell death and to preserve integrity of the tumor microenvironment and will directly implant it into NOD-SCID mouse (via subcutaneous on the flank of the mouse and or via sub renal capsule route). The NOD-SCID breed of mouse lacks Natural Killer cells and is considered more immunodeficient than a nude mouse. At the same time, a portion of the same tissue including adjacent normal tissue will be frozen and paraffin embedded for molecular verification (sequencing and IF to evaluate the preservation of histopathology, genome architecture, and global gene expression of donor tumors), hence ensuring the integrity of line.

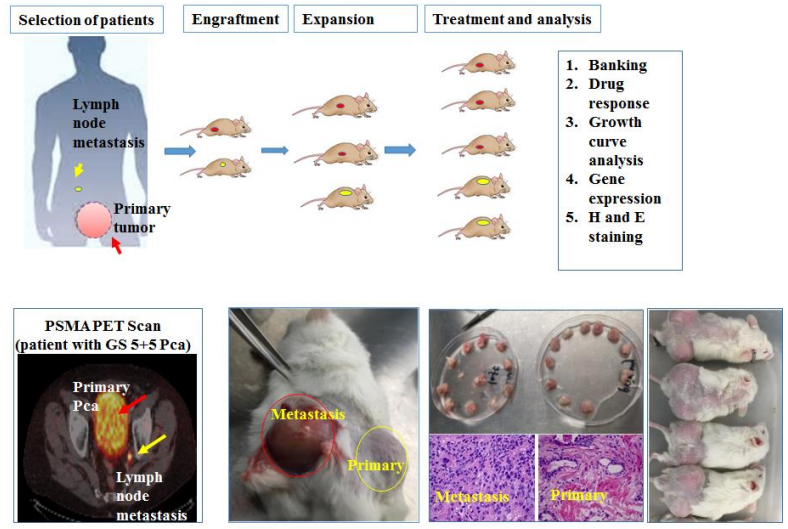

Figure 4. Establish a new cohort of Patient-Derived Xenografts (PDX) models to test the therapeutic for advance prostate cancer. A. At time of surgery, tumors from a patient with lymph node metastasis (identify on PSMA imaging) and known PTEN loss mutation (based on genomic profiling of pre-surgery biopsy sample) were implanted in the flank of NSG mouse. Successful lines are established once they can undergo passages and revival from cryopreservation. We verified the integrity of each passage by histopathological comparison to the original tumor.

To demonstrate the feasibility of developing patient derived xenograft models in the current research proposal, we successfully established of several lines of PDXs, wherein tumor xenografts were derived from a patient with pelvic lymph node metastasis found on PSMA PET scan (prostate specific membrane antigen positron emission tomography scan). These lines of PDXs were derived from high grade tumor. The limitation to establish successful PDX models for prostate cancer has been the low take rate. We have overcome these limitations by using advance imaging (PSMA PET) and tumor profiling (Decipher Grid, RNA seq) to identify aggressive tumor with specific mutations prior to implantation. We also have fast tracked the tissue preservation protocol to allow maximal preservation of tumor integrity to ensure

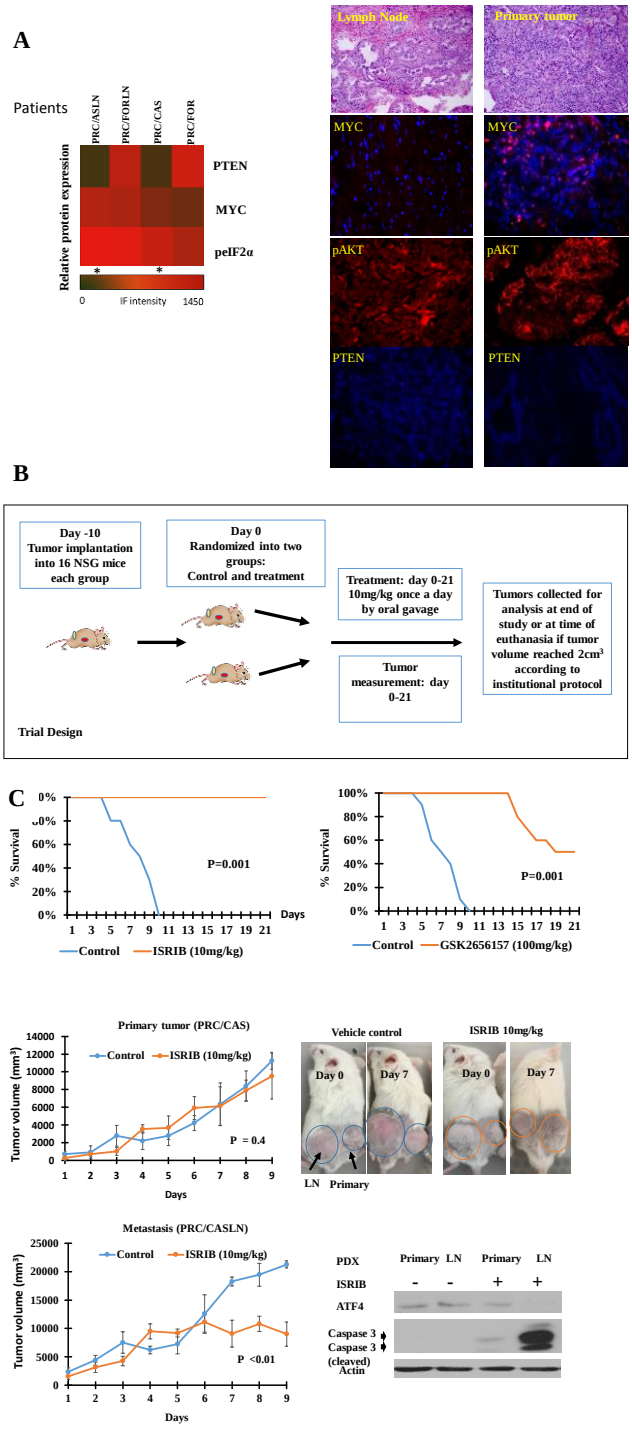

Figure 5. A new paradigm for selection of specific model of PDXs with hyperactivation of MYC and PTEN loss to interrogate novel pharmacogenomics approach to target a survival stress response pathway human prostate cancer. A. Heat map showing expression level of PTEN, MYC and phospho-eIF2a normalized to adjacent benign tissue as assess by quantitative immunofluorescence (left panel). Right panel showed detail IF staining of MYC, PTEN, phosphor AKT and H&E for the two line of PDXs, selected for the clinical. B. Upper panel showed trail design, lower panel showed Kaplan-Meier analysis of overall survival in the control and treated group (phospho-eIF2α inhibitor (ISRIB) and PERK inhibitor, (GSK2656157) N=16). C. Tumor volume is assessed daily in the placebo and ISRIB treated groups. Shown are representative picture of tumor at day 0 and day 9 following treatment. Western blot analysis of tumor following treatment showing expression of ATF4, a downstream target of eIF2α phosphorylation and cleaved caspase 3 level (apoptosis marker).

successful grafting. The PDX models are maintained by directly passing tumors from mouse to mouse once the tumor burden reached $2cm^3$. One advantage of using PDX models over cell-line derived xenografts is the ability create a library of PDXs with specific pathways that has been implicated in driving prostate tumorigenesis and progression (i.e. Myc driven, or PTEN-loss/MYC hyperactivation, AR signaling, SPOP, RAS/RAF).

In the current research program, we propose to establish a cohort of 20 different line of PDXs in the setting of diverse racial/ethnic background to best recapitulate the existing heterogeneity of prostate cancer in human. Once we accomplish this aim, a subsequent development of a proteomic array from these PDXs will provide an important resource to the scientific community in selecting specific models of prostate cancer for a particular therapeutic of interest. Within the context of our current proposal, the cohort of PDXs models should provide us the most comparable model of human prostate cancer to properly characterized the predicting responsiveness to targeted therapeutic benefit of inhibiting eIF2a phosphorylation and other UPR arms on the growth of primary human and metastatic prostate cancer. Once we have a library of 20 different PDXs established, we will also have access different subset model of prostate cancer to allow more specificity in selecting appropriate therapies when investigating novel therapeutics. Previous studies demonstrated the existence of gnomically distinct subtypes of prostate cancer and the variable clinical course ranging from indolence low grade cancer to very aggressive lethal prostate cancer. We will characterize each subtype of our PDX line using exome and whole genome DNA sequencing, RNA sequencing, miRNA sequencing, and protein arrays to provide a comprehensive profile of somatic copy-

number alterations, mRNA, microRNA, and protein levels for each distinct subtype of PDXs model of prostate cancer.

In the second part, we propose a new paradigm of personalized therapeutics to evaluate novel therapies targeting eIF2a phosphorylation and other UPR arms. In the proof of concept experiment, we selected two models from our current cohort of PDXs (unpublished) with the first PDX bearing tumor showing loss of PTEN expression and concurrently has low MYC expression at the protein level. The second PDX model has loss of PTEN with high MYC protein expression (Figure 5a). PTEN loss and MYC overexpression at the mRNA level as also validated using available genomic profiling of the tumor and exome DNA sequencing (data not shown). Furthermore, we observed that the high MYC/PTEN loss tumor displayed a significantly higher level of eIF2α phosphorylation over the low MYC/PTEN loss tumor using qualitative immunofluorescence analysis.

We subsequently evaluate the efficacy of ISRIB, a small molecule that specifically reverse the effect eIF2α phosphorylation on tumor growth and cancer specific survival (Kaplan Meir curve) as shown in Figure 2B. Here we designed a randomized trial with a line of PDX bearing MYC hyperactivation/PTEN loss tumors (N=8 mice in each groups and subjected them to treatment with placebo (control vehicle), GSK2656157 at 100mg/kg (inhibitor of PERK phosphorylation) or with ISRIB at 10mg/kg, a small molecule which reverses the effects of eIF2α phosphorylation. In the control vs ISRIB trial, we observed dramatic tumor reduction and a durable survival advantage (KM curve Fig 5a). In the control vs GSK2656157 trial, tumor regression was modest (data not shown) and cancer specific survival was extended but not durable in the GSK2656157 treated arm. Our data suggested that MYC hyperactivation/PTEN loss driven prostate cancer could converge at eIF2α phosphorylation, hence it is an excellent and specific window for therapeutic intervention.

We next evaluate whether ISRIB has selective efficacy across tumors with variable level of high or low eIF2α phosphorylation. In the PDX (PRC/CAS, primary tumor) with low level of eIF2α phosphorylation, there is no significant tumor regression at day 7 following ISRIB treatment whereas tumor (PRC/CASLN) with high eIF2α phosphorylation has dramatic regression in tumor volume, as well as increased cleaved caspase 3 level (Figure 5C) and decrease ATF-4 (a downstream event of eIF2α phosphorylation). Interestingly, ISRIB does not seem to produce a durable response in tumor regression in the PDX tumor with low eIF2α phosphorylation. Our data implicated that choosing a specific therapy for a distinct subset of prostate cancer is of utmost important to achieve a durable and effective response.

Given the finding that both PERK and IRE-1 arms of the UPR are activated upon MYC hyperactivation/PTEN loss, to this end we propose to test the efficacy of novel inhibitors for each arms of the UPR pathway using our PDX models. In the second preclinical trial when we treated mice bearing PDX, there is significant survival advantage in mice treated with PERK inhibitor (GSK2656157), however the survival advantage was not durable since 50% of mice treated with PERK inhibitor eventually demonstrated resistant and die from tumor progression at day 21 post treatment. This could be explained by the existence of a compensatory mechanism that resulted in upregulation of the IRE-1/XBP1 arms of the UPR in the setting of prolonged PERK inhibition. We will further examine the mechanism for this resistance by directly examine IRE/XPB-1 phosphorylation. *Is there a point downstream when both PERK and IRE-1 signaling converge? How does each arm of the UPR compensate when one is inhibited, Is there any a synergy in tumor regression when both inhibitors of the UPR are combined?* To address these questions, we will assess the therapeutic value of IRE/XBP-1 pathway inhibition in the PDXs model using a potent IRE-1 inhibitor. If there is a compensatory mechanism, inhibiting IRE-1/XBP1 with B-109 will demonstrate similar survival and tumor response profile as in the GSK2656157 treated group. Moreover, we have the potential to test a treatment strategy using a

combination of both PERK and IRE-1 inhibitors in the PDXs, prior to bringing them to human trial. We will also conduct a Kaplan-Meier survival analysis to assess whether the dual combination can completely prevent MYC/PTEN loss induced prostate cancer development.

What opportunities for training and professional development has the project provided?

- *With this physician training award, I was able to secure a position as assistant professor of urology in Residence. I successfully competed and won the 2016 Young Investigator Award from the Prostate Cancer Foundation. I presented my work at several national meeting including the PCF young investigator meeting, AUA western section and SUO annual meeting.*

- *I also directly supervise a post-doctoral fellow Crystal Conn PHD and trained research associate Lingru Xuei MS.*

- ***Professional development activities:*** *I am the PI for multi-institutional trial for PSMA imaging in active surveillance patients with low risk prostate cancer.* "A Phase 3 Study to Evaluate the Safety and Efficacy of 99mTc-MIP-1404 SPECT/CT Imaging to Detect Clinically Significant Prostate Cancer in Men With Biopsy Proven Low-Grade Prostate Cancer Who Are Candidates for Active Surveillance (proSPECT-AS)" I started the patient derived xenografts consortium at UCSF as a result *in increased knowledge or skill in one's area of expertise.*

- **How were the results disseminated to communities of interest?**

- *Early success of the PDX model that I started for this research grant had prompt a few collaborations in other discipline.*

  For instance, I am collaborating with Dr. Anwar (also recipient of the DOD physician training award) in vivo studies and evaluation of PSMA fluorescence imager as a novel imaging tool to detect microscopic residual tumor at tumor margin localize microscopic nodal disease not visualize by conventional imaging at time of tumor resection using patient-derived xenografts tumors with high PSMA expression. The purpose of study is to test the prototype imager on detecting microscopic tumor margin with 500 micro or larger and to evaluate the accuracy of the imager. The aim involves validation of PSMA- Fluorescently tagged anti-PSMA is injected preoperatively, and can be imaged intraoperatively. We then evaluate the biodistribution, toxicity and half-life of fluorescently tagged anti-PSMA injected in the PDX model. Finally, in we will evaluate the in vivo efficacy of imager on PDX mice and test for accuracy using immuno-histochemistry. These studies are greatly enabled by our lab's extensive experience developing PDX and characterizing other targeted therapy for prostate cancer. By targeting tumor tissue that is best to recapitulate prostatectomy in human, we used patient derived xenografts model of human prostate cancer resection. We hypothesize that imager will be able to accurate detect microscopic residual tumor after resection of primary tumor and that it will be highly efficacious in localizing microscopic disease in the lymph nodes that are located behind 5mm of normal tissue.

- **What do you plan to do during the next reporting period to accomplish the goals?**

  In the next report, I hope to to define the mechanism by which loss of PTEN and MYC hyperactivation alter mRNA translational networks associated with UPR activation and eIF2 phosphorylation to sustain tumor growth using ribosomal profiling and proteomic approaches. In addition, I will present data on **tissue array with 200 human prostate samples to interrogate how eIF2α phosphorylation and the other arms of the UPR pathway associate with worse clinical prognosis and survival outcomes.**

2. **IMPACT:**

Our hypothesis is that hyperactivation of mTOR and Myc induce a proteotoxic stress and cancer cells activate a survival adaptive response pathway to increase cellular fitness and tumor growth. Our genetically and pharmacologically preliminary data showed that upon UPR activation and phosphorylation of eIF2a downregulate protein synthesis rate, represents a new point of vulnerability of primary and metastatic prostate cancer cells. We next seek to understand the molecular mechanisms of specific protein expression program that steer key cellular hallmarks underling prostate cancer development and to develop a novel therapeutic regimen to target a new point of vulnerability of prostate cancer cells dependent on eIF2a survival and UPR stress response pathway. Delineating the mechanisms underlying stress response pathways, in particular the unfolded protein response (UPR), in novel mouse models (MYC hyperactivation/PTEN knock down) and human prostate cancer using PDX models will lead to novel therapies to target stress response pathways.

What was the impact on the development of the principal discipline(s) of the project?

- *Nothing to Report*
- **What was the impact on other disciplines?**
- *Nothing to Report*
- **What was the impact on technology transfer?**
- *The development of PDX (patient derived xenografts) for primary and metastatic prostate cancer could be a useful technology to allow quick and effective way to evaluate new therapy or imaging modality for prostate cancer.*
-
- **What was the impact on society beyond science and technology?**
- *Nothing to Report*

3. **CHANGES/PROBLEMS:**

Nothing to Report

- **Changes that had a significant impact on expenditures**
- *Nothing to report*
- **Significant changes in use or care of human subjects, vertebrate animals, biohazards, and/or select agents**
- Nothing to report
- **Significant changes in use or care of human subjects**
- **Significant changes in use or care of vertebrate animals.**

Significant changes in use of biohazards and/or select agents

4. **PRODUCTS:**

Nothing to Report.

- **Publications, conference papers, and presentations**

- **Journal publications.**

- *Hsieh AC, Nguyen HG, Wen L, Edlind MP, Carroll PR, Kim W, Ruggero D. Cell type-specific abundance of 4EBP1 primes prostate cancer sensitivity or resistance to PI3K pathway inhibitors. Sci Signal. 2015; 8(403):ra116. PMID: 26577921. Federal support (yes).*

- **Books or other non-periodical, one-time publications.**

- **Other publications, conference papers, and presentations.**

- **Website(s) or other Internet site(s)**
  Technologies or techniques
  *Novel method for PDX generation: W*e successfully established of several lines of PDXs, wherein tumor xenografts were derived from a patient with pelvic lymph node metastasis found on PSMA PET scan (prostate specific membrane antigen positron emission tomography scan). These lines of PDXs were derived from high grade tumor. The limitation to establish successful PDX models for prostate cancer has been the low take rate. We have overcome these limitations by using advance imaging (PSMA PET) and tumor profiling (Decipher Grid, RNA seq) to identify aggressive tumor with specific mutations prior to implantation. We also have fast tracked the tissue preservation protocol to allow maximal preservation of tumor integrity to ensure successful grafting. *These PDX will be shared among the research community.*

- **Inventions, patent applications, and/or licenses**
  nothing to report

  Other Products

  Nothing to report

5. **PARTICIPANTS & OTHER COLLABORATING ORGANIZATIONS**

- **What individuals have worked on the project?**

- *no change*

- **Has there been a change in the active other support of the PD/PI(s) or senior/key personnel since the last reporting period?**

- *Nothing to Report*

- **What other organizations were involved as partners?**

- *Nothing to Report*

6. **SPECIAL REPORTING REQUIREMENTS**

Nothing to report

7. **APPENDICES:**

8. ***Reprints of journal article and CV***

****
********** **ADDITIONAL NOTES:**

CANCER

Cell type–specific abundance of 4EBP1 primes prostate cancer sensitivity or resistance to PI3K pathway inhibitors

Andrew C. Hsieh,[1,2*†‡] Hao G. Nguyen,[1§] Lexiaochuan Wen,[1§] Merritt P. Edlind,[1] Peter R. Carroll,[1] Won Kim,[2] Davide Ruggero[1,3‡]

Pharmacological inhibitors against the PI3K-AKT-mTOR (phosphatidylinositol 3-kinase–AKT–mammalian target of rapamycin) pathway, a frequently deregulated signaling pathway in cancer, are clinically promising, but the development of drug resistance is a major limitation. We found that 4EBP1, the central inhibitor of cap-dependent translation, was a critical regulator of both prostate cancer initiation and maintenance downstream of mTOR signaling in a genetic mouse model. 4EBP1 abundance was distinctly different between the epithelial cell types of the normal prostate. Of tumor-prone prostate epithelial cell types, luminal epithelial cells exhibited the highest transcript and protein abundance of 4EBP1 and the lowest protein synthesis rates, which mediated resistance to both pharmacologic and genetic inhibition of the PI3K-AKT-mTOR signaling pathway. Decreasing total 4EBP1 abundance reversed resistance in drug-insensitive cells. Increased 4EBP1 abundance was a common feature in prostate cancer patients who had been treated with the PI3K pathway inhibitor BKM120; thus, 4EBP1 may be associated with drug resistance in human tumors. Our findings reveal a molecular program controlling cell type–specific 4EBP1 abundance coupled to the regulation of global protein synthesis rates that renders each epithelial cell type of the prostate uniquely sensitive or resistant to inhibitors of the PI3K-AKT-mTOR signaling pathway.

INTRODUCTION

The PI3K-AKT-mTOR (phosphatidylinositol 3-kinase–AKT–mammalian target of rapamycin) signaling pathway is altered in 100% of advanced human prostate cancer patients, which is a disease that arises from the prostatic epithelium composed of two distinct epithelial cell types, luminal and basal epithelial cells (*1*). Both cell types can transform and develop into tumors in the context of various oncogenic stimuli. For example, loss of PTEN (phosphatase and tensin homolog), the tumor suppressor and negative regulator of the PI3K-AKT-mTOR signaling pathway, leads to tumor development in either cell type in mouse models of prostate cancer (*2*). Others have shown that overexpression of the kinase AKT and the transcription factor MYC in normal basal epithelial cells leads to the formation of a luminal-like prostate cancer (*3*). Moreover, loss of PTEN within a prostate luminal epithelial stem cell population also leads to tumorigenesis in vivo (*4*). These findings demonstrate that multiple cancer-initiating cell types exist within the prostate and that tumor initiation can be driven by oncogenic PI3K-AKT-mTOR activity. However, an important unanswered question is whether all prostate tumor epithelial cell types are equally sensitive to inhibitors of the PI3K pathway or are specific cell types primed for drug resistance. This is a critical question because an emerging problem shared by all PI3K pathway inhibitors is drug resistance, which is significantly stifling the clinical success of this class of therapeutic agents.

The kinase mTOR promotes mRNA translation by converging on the eIF4F (eukaryotic translation initiation factor 4F) cap-binding complex, which is a critical nexus that controls global protein synthesis as well as the translation of specific mRNA targets (*5*–*7*). All eIF4F complex members including the cap-binding protein and oncogene eIF4E (*8*, *9*), the scaffolding molecule eIF4G (*10*), and the RNA helicase eIF4A (*11*) are required for cap-dependent translation. The eIF4F complex is negatively regulated by a critical interaction between eIF4E and the tumor suppressor eIF4E-binding proteins (4EBPs), which are phosphorylated and inhibited by mTOR (*6*, *12*). Using unique mouse models of prostate cancer, we addressed the important question of cell type specificity and translation control in tumor initiation, cancer progression, and drug resistance, and found that 4EBP1 activity is not only a marker of PI3K-AKT-mTOR signaling but is also critical for prostate cancer initiation and maintenance as well as the therapeutic response. We found that a specific population of tumor-forming luminal epithelial cells, which exhibit high transcript and protein levels of 4EBP1 and low protein synthesis rates, is remarkably resistant to inhibition of the PI3K-AKT-mTOR signaling pathway. Furthermore, we found that elevated 4EBP1 expression is necessary and sufficient for drug resistance. Using patient samples acquired from a phase 2 clinical trial with the oral pan-PI3K inhibitor BKM120, we found that a high amount of 4EBP1 protein was a characteristic of posttreatment prostate cancer cells. Together, our findings reveal a normal cellular program characterized by high 4EBP1 abundance and low protein synthesis rates in luminal epithelial cells that can be exploited by prostate cancer to direct tumor growth in the context of PI3K pathway inhibition.

[1]Department of Urology, University of California, San Francisco, San Francisco, CA 94158, USA. [2]Division of Hematology/Oncology and Department of Internal Medicine, University of California, San Francisco, San Francisco, CA 94158, USA. [3]Department of Cellular and Molecular Pharmacology, University of California, San Francisco, San Francisco, CA 94158, USA.
*Present address: Division of Human Biology, Fred Hutchinson Cancer Research Center, Seattle, WA 98109, USA.
†Present address: Department of Medicine, University of Washington, Seattle, WA 98195, USA.
‡Corresponding author. E-mail: ahsieh@fredhutch.org (A.C.H.); davide.ruggero@ucsf.edu (D.R.)
§These authors contributed equally to this work.

RESULTS

Luminal epithelial cells with increased 4EBP1 abundance define a PI3K-AKT-mTOR pathway inhibitor–resistant cell type in vivo

PI3K-AKT-mTOR pathway inhibitors have demonstrated significant preclinical efficacy in prostate cancer preclinical trials; however, drug resistance

inevitably develops (*13*). Multiple prostate epithelial cell types have been implicated in tumorigenesis, including luminal epithelial cells and basal epithelial cells (*2*); however, it is unknown if both cell types are equally sensitive to PI3K-AKT-mTOR pathway inhibition or if specific cell types are more resistant than others. We previously conducted a preclinical trial with the adenosine 5′-triphosphate (ATP) site mTOR inhibitor MLN0128 (*7*) in mice that develop prostate cancer through loss of the tumor suppressor PTEN in both basal and luminal epithelial cells (herein referred to as $PTEN^{L/L}$) (*14*). Although we observed a decrease in the amount of prostate tumors, we also observed that a significant number of tumors remained despite an 8-week therapeutic course with MLN0128 (*7*). To characterize the prostate cancer epithelial cell types prone to drug resistance, we quantified the number of basal epithelial cells and luminal epithelial cells that remained in $PTEN^{L/L}$ mice treated with MLN0128 (*7*). After an 8-week treatment course with MLN0128 or vehicle, the tumors that remained in $PTEN^{L/L}$ mice treated with MLN0128 were enriched for $CK8^+$ luminal epithelial cells over $CK5^+$ basal epithelial cells (Fig. 1A and fig. S1, A and B). These findings suggest that tumor-forming luminal epithelial cells are more resistant than basal epithelial cells to inhibition of the PI3K-AKT-mTOR signaling pathway.

Next, we sought to determine the molecular features of resistant luminal epithelial cells that differentiate them from basal cells. The 4EBP1-eIF4E axis is a critical downstream target of mTOR that mediates the therapeutic efficacy of ATP site mTOR inhibitors (*15*). Hence, we sought to determine the abundance of 4EBP1 and each of the eIF4F components (eIF4E, eIF4A, and eIF4G) in both luminal and basal epithelial cells. To this end, we sorted luminal and basal epithelial cells from wild-type and $PTEN^{L/L}$ mice treated with and without MLN0128 and Western-blotted for pathway components. We used the cell surface marker and integrin CD49f and the murine stem cell marker Sca-1 to distinguish luminal epithelial cells from basal epithelial cells (*16*). In particular, wild-type and $PTEN^{L/L}$ basal epithelial cells are CD49f- and Sca-1–high, and luminal epithelial cells are CD49f positive and Sca-1–low, which was confirmed by quantitative polymerase chain reaction (qPCR) analysis of their respective markers on sorted cell populations (fig. S2, A and B) (*16*). Loss of PTEN and hyperphosphorylation of AKT were confirmed by qPCR, Western blot analysis, and immunofluorescence in $PTEN^{L/L}$ basal and luminal epithelial cells (fig. S3, A to C). Among all the translation initiation components analyzed, only 4EBP1 protein levels were increased in $PTEN^{L/L}$ luminal epithelial cells in both MLN0128-treated and untreated mice (Fig. 1, B and C). Notably, the phosphorylation of 4EBP1 was similar in basal and luminal epithelial cells and therefore do not contribute to the differences seen in total 4EBP1 abundance (Fig. 1B and fig. S3D). Moreover, we did not observe nuclear sequestration of 4EBP1 or cytoplasmic foci of 4EBP1 in luminal cells compared to basal cells (fig. S3E). The abundance of eIF4A and eIF4E was equivalent between treated and nontreated luminal and basal epithelial cells (Fig. 1B), whereas the abundance of eIF4G exhibited only a mild decrease in luminal epithelial cells compared to basal epithelial cells (Fig. 1B). Together, these findings reveal that luminal epithelial cells, which we found to be prone to drug resistance, are characterized by high abundance of the translational repressor 4EBP1.

Prostate epithelial cells have distinct amounts of *4EBP1* mRNA expression that underlies cell type–specific protein synthesis rates within the prostate

We next asked whether the higher amounts of 4EBP1 in prostate luminal epithelial cells were the result of PTEN loss or instead reflect a normal expression program. Unexpectedly, we found that 4EBP1 protein abundance

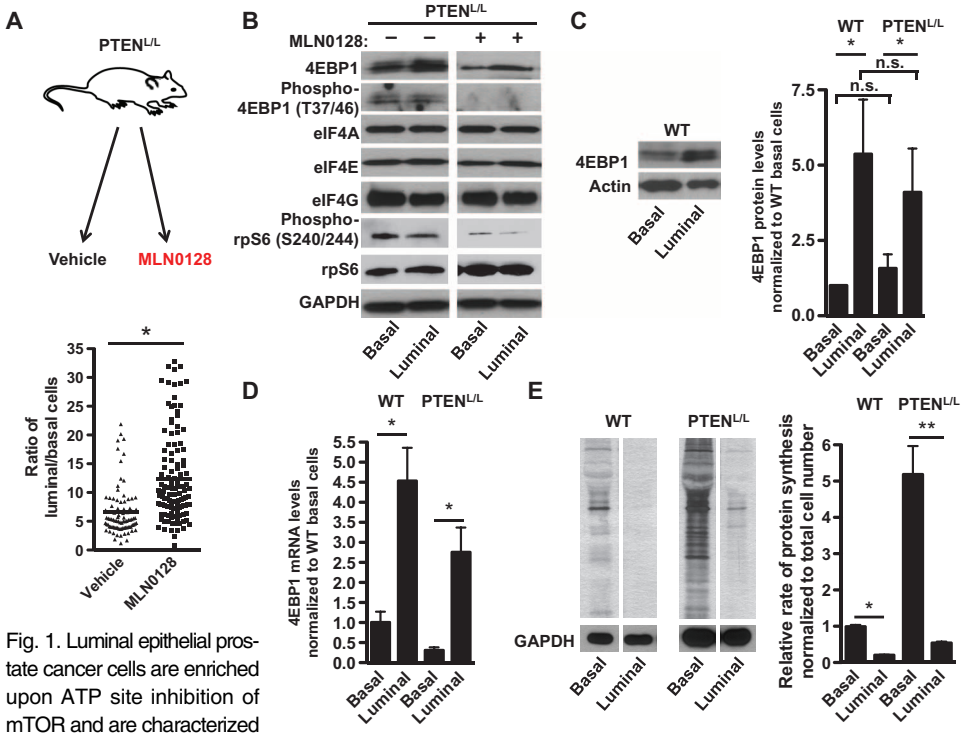

Fig. 1. Luminal epithelial prostate cancer cells are enriched upon ATP site inhibition of mTOR and are characterized by increased 4EBP1 protein abundance and lower baseline protein synthesis rates in vivo. (**A**) Schematic of MLN0128 preclinical trial. Age-matched 9- to 12-month-old $PTEN^{L/L}$ mice were treated with vehicle or MLN0128 (1 mg/kg) daily for 8 weeks (upper panel). Quantification for ratio of $CK8^+$ luminal epithelial cells over $CK5^+$ basal epithelial cells in vehicle- or MLN0128-treated $PTEN^{L/L}$ mice (lower panel; $n = 6$ mice per condition; $^*P < 0.05$, *t* test). (**B**) Representative Western blots for 4EBP1, eIF4A, eIF4E, eIF4G, phospho-4EBP1 ($Thr^{37/46}$), phospho–rpS6 (ribosomal protein S6) ($Ser^{240/244}$), and rpS6 in basal epithelial and luminal epithelial cells from $PTEN^{L/L}$ mice treated with and without MLN0128 (1 mg/kg) daily for 4 days by oral gavage. (**C**) Representative Western blot for 4EBP1 in basal epithelial and luminal epithelial cells from wild-type (WT) mice (left panel). Quantification of 4EBP1 densitometry in both WT and $PTEN^{L/L}$ basal and luminal epithelial cells (right panel; $n = 3$ mice per genotype; $^*P = 0.04$, *t* test). (**D**) *4EBP1* mRNA expression in WT and $PTEN^{L/L}$ basal and luminal epithelial cells ($n = 2$ to 3 mice per genotype; $^*P = 0.002$, *t* test). All samples were first normalized to actin. (**E**) Representative [^{35}S]methionine incorporation run on the same gel in sorted basal and luminal epithelial cell types from WT and $PTEN^{L/L}$ mice (left panel). Quantification of [^{35}S]methionine incorporation by densitometry in sorted basal and luminal epithelial cell types from WT and $PTEN^{L/L}$ mice (right panel; $n = 3$ mice per genotype; $^*P < 0.0001$, $^{**}P = 0.002$, *t* test). Data are means ± SEM. GAPDH, glyceraldehyde-3-phosphate dehydrogenase; n.s., not significant.

was considerably higher in wild-type luminal epithelial cells compared to that in wild-type basal epithelial cells (Fig. 1C). To determine at what level of gene expression 4EBP1 is regulated in luminal and basal epithelial cells, we conducted qPCR analysis of *4EBP1* expression in both cell types from wild-type and $PTEN^{L/L}$ mice. *4EBP1* mRNA expression was three- to fivefold higher in normal and $PTEN^{L/L}$ luminal epithelial cells compared to basal epithelial cells, revealing differential transcriptional regulation of 4EBP1 in distinct tumor-prone prostate epithelial cell types (Fig. 1D).

Next, we sought to determine the functional relevance of increased 4EBP1 transcript and protein amounts in luminal epithelial cells. 4EBP1 is a negative regulator of cap-dependent translation and has been shown to decrease the rate of protein synthesis (*12*). We therefore conducted [^{35}S] methionine incorporation assays on fluorescence-activated cell sorting (FACS)–sorted basal and luminal epithelial cells from wild-type and $PTEN^{L/L}$ mice to determine the baseline mRNA translation rates in each cell type. The rates of de novo protein synthesis between the two cell types were significantly different, with basal epithelial cells exhibiting a markedly greater amount of protein synthesis than luminal epithelial cells (Fig. 1E). To determine whether other translation components besides 4EBP1 may contribute to the difference in protein synthesis rates between basal and luminal epithelial cells, we conducted a candidate protein expression analysis of major regulators of translation, including the phosphorylation of eEF2 (eukaryotic elongation factor 2), eIF2α, rpS6 and the abundance of the translation initiation inhibitors 4EBP2 and PDCD4 (programmed cell death protein 4). The phosphorylation of eEF2 and eIF2α was similar in both cell types in the $PTEN^{L/L}$ with no changes in total abundance of eEF2 or eIF2α (fig. S4). Phosphorylation of rpS6, which has an inhibitory effect on protein synthesis (*17*), was decreased in luminal epithelial cells compared to basal epithelial cells (Fig. 1B). The abundance of both 4EBP2 and PDCD4 was decreased in $PTEN^{L/L}$ luminal epithelial cells compared to that in basal epithelial cells (fig. S4). Hence, the phosphorylation status of eEF2, eIF2α, and rpS6 and the protein abundance of 4EBP2 and PDCD4 cannot account for the difference in protein synthesis rates observed between $PTEN^{L/L}$ basal and luminal epithelial cells.

Despite having similarly increased abundance of 4EBP1 as $PTEN^{L/L}$ luminal epithelial cells, wild-type luminal epithelial cells displayed the lowest protein synthesis rates compared to all other cell types studied. This suggests that other factors besides 4EBP1 abundance may further limit wild-type luminal epithelial cell protein synthesis rates. For example, we observed that eIF2α phosphorylation was slightly increased in wild-type luminal epithelial cells compared to basal epithelial cells (fig. S4). This increase was not observed in $PTEN^{L/L}$ luminal cells and therefore cannot account for drug resistance or the low protein synthesis rates in the transformed setting (fig. S4). Thus, prostate epithelial cell types were distinguished by their innate protein synthesis rates, which inversely correlated with 4EBP1 transcript and protein amounts and may underlie MLN0128 resistance. Moreover, these findings suggest that a transcriptional program, which dictates the cell type–specific expression of *4EBP1*, may control the differential protein synthesis rates between basal and luminal epithelial cells. The molecular program that governs prostate epithelial cell–specific *4EBP1* expression remains a question for future investigation.

The 4EBP1-eIF4E axis is a critical driver of prostate cancer initiation and maintenance downstream of mTOR

Although in vitro work has demonstrated the importance of eIF4E activity in prostate cancer cell lines (*18*–*20*), little is known about the role of 4EBP1 in prostate cancer initiation and progression in vivo. Given the striking difference in *4EBP1* expression within the normal prostate, we next asked whether eIF4E hyperactivity is a critical driver of prostate cancer development as well as the therapeutic response or resistance of specific epithelial cell types. To directly address this question, we developed a genetic model in which eIF4E activity can be inhibited within all prostate epithelial cell types in an inducible fashion. In this model (Fig. 2A), the probasin (PB) promoter drives Cre recombinase expression (*21*) and prostate-specific recombination of a lox-stop-lox (LSL) element, which precedes a reverse tetracycline-controlled transactivator gene (rtTA) within the Rosa26 locus (*22*). In the presence of the tetracycline analog doxycycline, the rtTA drives the expression of a tetracycline-responsive mutant form of 4EBP1 (TetO-$4EBP1^{M}$) in which all the mTOR-sensitive phosphorylation sites have been mutated to alanine. We previously used the mTOR-insensitive mutant $4EBP1^{M}$ to decrease eIF4E hyperactivation in vivo in hematologic cancers (*15*). Using this mouse model, we studied the effects of the TetO-$4EBP1^{M}$ in normal prostate epithelial cells. We induced the expression of $4EBP1^{M}$ in PB-$Cre^{Tg/+}$;Rosa-LSL-$rtTA^{KI/KI}$;TetO-$4EBP1^{M/M}$ (herein referred to as $4EBP1^{M}$) mice at weaning before the onset of male puberty for 4 to 5 weeks with doxycycline (fig. S5A) (*23*). We verified transgene expression and found that the prostate glands of $4EBP1^{M}$-induced mice exhibited no histological differences compared to wild-type mice (Fig. 2B and fig. S5, B and C). Thus, $4EBP1^{M}$ expression does not affect normal prostate gland development or histological features of a mature murine prostate.

To genetically determine the role of eIF4E hyperactivity toward prostate tumorigenesis and cancer progression, we developed the PB-$Cre^{Tg/+}$;$PTEN^{L/L}$;Rosa-LSL-$rtTA^{KI/KI}$;TetO-$4EBP1^{M/M}$ mouse model (herein referred to as $PTEN^{L/L}$;$4EBP1^{M}$). In this system, loss of the PTEN tumor suppressor drives PI3K-AKT-mTOR signaling, hyperactivation of eIF4E, and subsequent development of preinvasive PIN lesions by 10 weeks of age (*14*). Administration of doxycycline induces the expression of the $4EBP1^{M}$ transgene (Fig. 2A), thereby decreasing eIF4E hyperactivation (*15*). Expression of $4EBP1^{M}$ within the prostate did not affect the ability of mTOR to phosphorylate other downstream targets such as the p70S6K1 and p70S6K2 target rpS6 (fig. S5D). $PTEN^{L/L}$ and $PTEN^{L/L}$;$4EBP1^{M}$ mice were placed on doxycycline for 4 to 5 weeks immediately after weaning and analyzed for the effects on tumor initiation (fig. S5A). Loss of PTEN caused a twofold increase in prostate size that was significantly blunted in $PTEN^{L/L}$;$4EBP1^{M}$ mice (fig. S5E). At a histological level, the $4EBP1^{M}$ transgene markedly inhibited the development of PIN in $PTEN^{L/L}$;$4EBP1^{M}$ mice (Fig. 2C), which complements a previous finding that eIF4E phosphorylation is necessary for prostate cancer development (*24*). Next, we sought to delineate the cellular mechanism underlying the tumor suppressive effects of $4EBP1^{M}$ expression. Confirming previously published work, $PTEN^{L/L}$ mice exhibited increased baseline amounts of both proliferation and apoptosis compared to wild-type mice (Fig. 2D and fig. S5F) (*14*). However, inhibition of eIF4E hyperactivity substantially increased apoptosis by fivefold (Fig. 2D), while having no effect on cell proliferation (fig. S5F), demonstrating that increased activity of eIF4E promotes a prosurvival program that is critical for tumor initiation.

Given the significant therapeutic potential of targeting eIF4E hyperactivity in established cancers, we used the inducible nature of the $PTEN^{L/L}$;$4EBP1^{M}$ mouse model to test the effect of eIF4E inhibition on tumor maintenance. $PTEN^{L/L}$ and $PTEN^{L/L}$;$4EBP1^{M}$ mice were aged to 7 to 9 months, corresponding to the development of large prostate tumors that can be visualized by ultrasound. At that point, mice were imaged before and after 8 weeks of doxycycline administration (fig. S5G). By the end of the trial, $PTEN^{L/L}$;$4EBP1^{M}$ mouse prostates were 50% smaller than those of $PTEN^{L/L}$ mice (Fig. 2, E and F). Moreover, whereas $PTEN^{L/L}$ mice exhibited a twofold increase in tumor area, $PTEN^{L/L}$;$4EBP1^{M}$ tumors exhibited no growth but instead a slight decline in tumor area (Fig. 2, G and H), which was associated with a threefold increase in apoptosis (Fig. 2I). Together, these findings provide in vivo evidence that eIF4E hyperactivity is critical for prostate cancer initiation and maintenance, and provide clinical

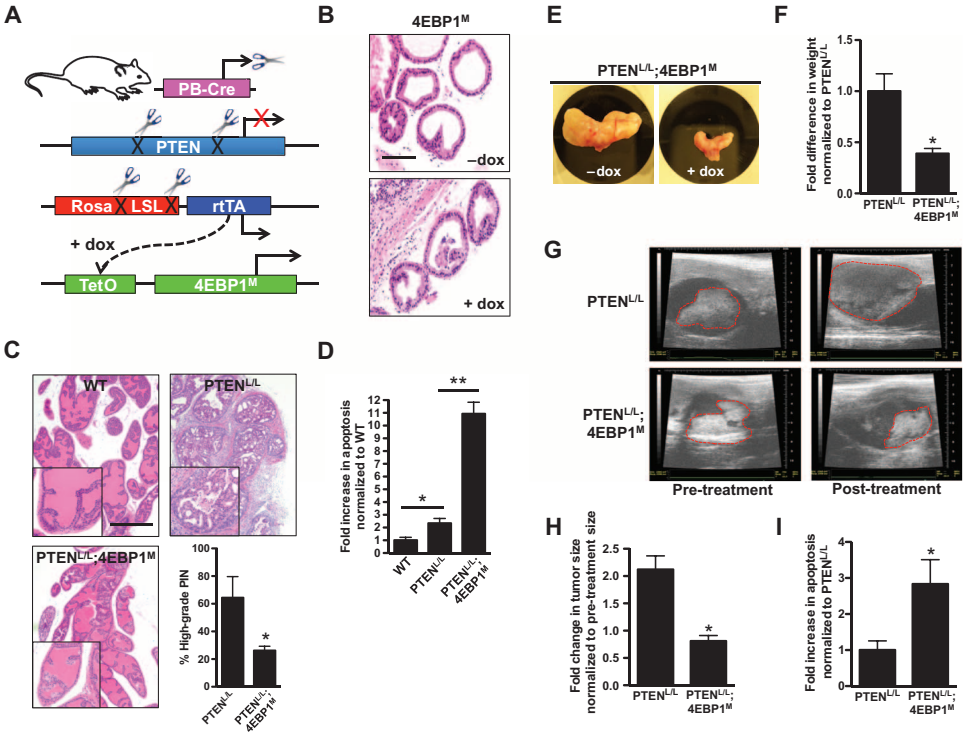

Fig. 2. Inhibition of eIF4E activity does not affect WT prostate epithelial cell maintenance but suppresses prostate tumor initiation and progression in the setting of *PTEN* loss in vivo. (A) Schematic representation of the prostate-specific and doxycycline-inducible PTEN$^{L/L}$;4EBP1^{M} mouse model, in which the addition of doxycycline (dox) to the drinking water (at 2 g/liter) induced the expression of the 4EBP1^{M} transgene. (B) Representative hematoxylin and eosin (H&E) staining of ventral prostate glands from 4EBP1^{M} mice after 4 weeks with or without doxycycline in their drinking water. Scale bar, 100 μm. (C) Representative H&E staining of WT, PTEN$^{L/L}$, and PTEN$^{L/L}$;4EBP1^{M} prostates after 4 to 5 weeks of exposure to doxycycline after weaning. Percent high-grade prostatic intraepithelial neoplasia (PIN)–positive glands in PTEN$^{L/L}$ and PTEN$^{L/L}$;4EBP1^{M} mice (n = 3 mice per genotype, $^{*}P$ = 0.03, t test). Scale bar, 500 μm. (D) Fold change in TUNEL (terminal deoxynucleotidyl transferase–mediated deoxyuridine triphosphate nick end labeling)–positive cells in WT, PTEN$^{L/L}$, and PTEN$^{L/L}$;4EBP1^{M} prostates after 4 to 5 weeks of exposure to doxycycline after weaning (n = 3 mice per genotype; $^{*}P$ = 0.004, $^{**}P$ < 0.0001, t test). (E) Representative PTEN$^{L/L}$;4EBP1^{M} prostate with or without exposure to doxycycline for 8 weeks starting at age 6 to 8 months. Mice were at 8 to 10 months of age at necropsy. (F) Quantification of mouse prostate weights between PTEN$^{L/L}$ and PTEN$^{L/L}$;4EBP1^{M} exposed to doxycycline for 8 weeks (n = 4 to 5 mice per genotype; $^{*}P$ = 0.02, t test). (G) Representative ultrasounds of PTEN$^{L/L}$ and PTEN$^{L/L}$;4EBP1^{M} anterior prostates before and after 8 weeks of exposure to doxycycline. (H) Quantification of tumor area in PTEN$^{L/L}$ and PTEN$^{L/L}$;4EBP1^{M} anterior prostates before and after 8 weeks of exposure to doxycycline (n = 4 to 5 mice per genotype; $^{*}P$ = 0.003, t test). (I) Fold change in TUNEL-positive (apoptotic) cells in PTEN$^{L/L}$ and PTEN$^{L/L}$;4EBP1^{M} (n = 3 mice per genotype; $^{*}P$ = 0.0006, t test). Data are means ± SEM.

precedence for therapeutically targeting upstream regulators of the translation initiation machinery, such as mTOR, in epithelial cancers.

PTEN$^{L/L}$ luminal epithelial cells are resistant to inhibition of eIF4E activity

Our genetic studies reveal that despite the marked effect of restraining eIF4E hyperactivity on prostate cancer development, this effect is incomplete, and certain prostate cancer cell populations continue to grow (Fig. 2G). This genetic effect was mirrored by what we observed after MLN0128 treatment, where a population of luminal epithelial cells was enriched after treatment (Fig. 1A). We therefore asked whether a specific population of prostate epithelial cells in PTEN$^{L/L}$;4EBP1^{M} mice may be less sensitive to the expression of the 4EBP1^{M} transgene. To address this question, we determined the change in the number of PTEN$^{L/L}$ luminal epithelial cells compared to PTEN$^{L/L}$ basal epithelial cells after the induction of the 4EBP1^{M} by both immunofluorescence and FACS. In the setting of PTEN loss (fig. S3, A and B), both basal and luminal epithelial cell populations increased in total number compared to wild-type cells and were characterized by increased entry into the cell cycle (fig. S6A), demonstrating the mitogenic effects of increased PI3K-AKT-mTOR pathway activation (Fig. 3A). Strikingly, however, we found that luminal epithelial cells were specifically enriched upon inhibition of eIF4E by the 4EBP1^{M}, which phenocopied our pharmacological findings with MLN0128 (Figs. 1A and 3B, and fig. S6, B to D). These findings suggest that eIF4E may be critical to transform basal epithelial cells, whereas luminal cells do not rely on increased eIF4E activation for their growth.

To elucidate the cellular mechanism that enables this divergent response in basal and luminal epithelial cells to inhibition of eIF4E activity, we conducted in vivo analysis of cell proliferation and apoptosis. Induction of the TetO-4EBP1^{M} transgene did not affect cell proliferation as determined by BrdU incorporation in any of the cell types in PTEN$^{L/L}$ mice (Fig. 3C). However, 4EBP1^{M} expression increased apoptosis in basal cells but did not affect luminal epithelial cells (Fig. 3D and fig. S6E). Hence, despite having tumorigenic potential in the context of PTEN loss, luminal epithelial cells are not dependent on eIF4E activity for cell survival, which underscores a surprising specificity in cell identity and sensitivity to inhibition of eIF4E activity in prostate cancer. These findings are consistent with the overall marked increase in *4EBP1* transcript expression and decreased protein synthesis rates in luminal compared to basal epithelial cells. Together, these findings suggest that the high protein synthesis rates normally exhibited by prostate basal cells prime them to be more vulnerable to eIF4E down-regulation in the oncogenic setting. These findings have further therapeutic implications because cells that normally exhibit higher *4EBP1* transcript expression may be more resistant to pharmacological inhibition of the PI3K signaling pathway.

Increased 4EBP1 abundance controls the rate of protein synthesis and drives resistance to PI3K-AKT-mTOR pathway inhibition in human prostate cancer cells

To determine whether increased abundance of 4EBP1 primes cells for resistance to PI3K-AKT-mTOR pathway inhibition, we developed a human prostate cancer cell line characterized by knockdown of PTEN and overexpression

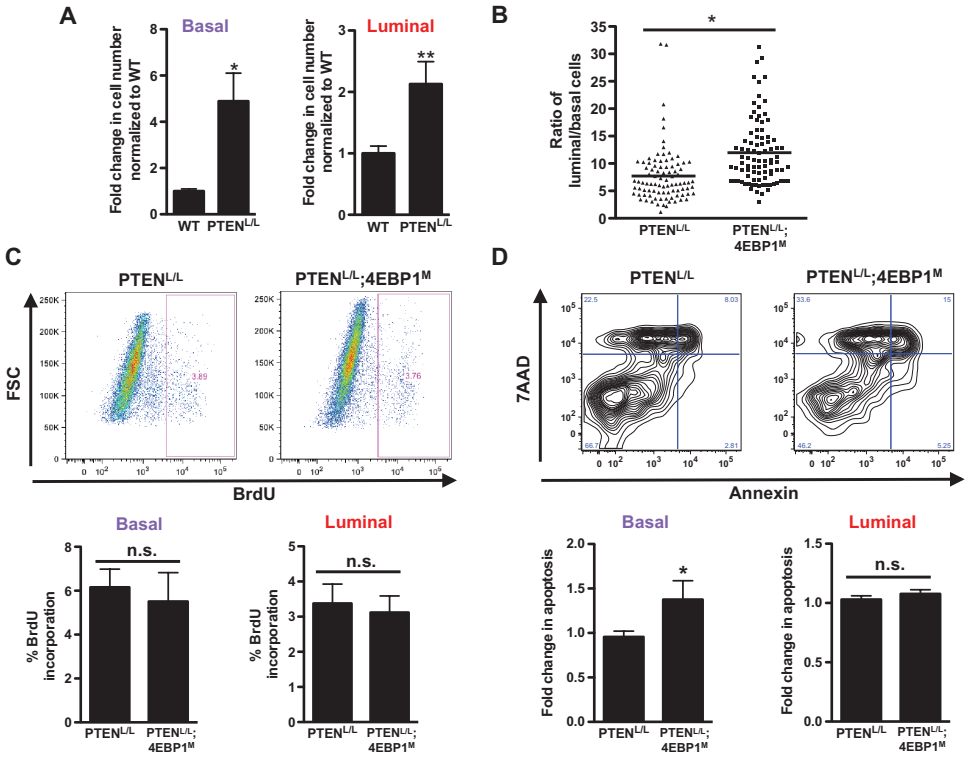

Fig. 3. PTEN$^{L/L}$ luminal epithelial cells are enriched upon expression of 4EBP1^{M}. (A) Fold change in basal and luminal epithelial cell numbers upon *PTEN* loss in WT and PTEN$^{L/L}$ mice (n = 7 to 9 mice per genotype; *P = 0.005, **P = 0.01, t test). (B) Ratio of CK8^{+} luminal epithelial cells over CK5^{+} basal epithelial cells in PTEN$^{L/L}$ and PTEN$^{L/L}$;4EBP1^{M} mice (n = 6 mice per condition; *P = 0.001, t test). (C) Percent 5-bromo-2′-deoxyuridine (BrdU) incorporation by FACS of the basal and luminal epithelial cell types from mice exposed to doxycycline (administered in the drinking water at 2 g/liter) at weaning for a total of 4 to 5 weeks. Upper: Representative BrdU dot plot. Lower: Quantification of percent BrdU-positive basal and luminal cells in each mouse strain (n = 5 to 6 mice per genotype, t test). FSC, forward scatter. (D) 7AAD/annexin FACS for apoptosis in basal and luminal epithelial cell types from mice exposed to the doxycycline regimen upon weaning for a total of 4 to 5 weeks. Upper: Representative 7AAD/annexin zebra plot. Lower: Quantification of 7AAD/annexin double-positive cells in basal or luminal cells in each mouse strain (n = 6 to 7 mice per genotype; *P = 0.03, t test). All mice were at 8 to 10 weeks of age at necropsy. Data are means ± SEM.

of large/small T antigen and human telomerase reverse transcriptase (hTERT) in primary prostate epithelial cells (PTEN KD LHS PrECs) (fig. S7A) (*25*). These cells exhibit important similarities with human prostate cancer, including the expression of luminal epithelial markers and the ability to form colonies in clonogenic growth assays (fig. S7, A and B). Similar to our pharmacologic and genetic studies, these cells also exhibited a heterogeneous response to treatment with MLN0128 characterized by populations of sensitive and primary resistant cells. To determine whether 4EBP1 abundance defines the resistant cell type, single-cell clones were isolated, characterized for their baseline 4EBP1 protein abundance, and treated with MLN0128 to determine the effects on cell survival by propidium iodide staining and annexin V analysis by FACS. We found that despite having similar loss of PTEN, individual clones had varying amounts of 4EBP1 mRNA and protein amounts (Fig. 4A and fig. S7C). Moreover, we observed that clones with lower 4EBP1 protein abundance were more sensitive to MLN0128 treatment, whereas those with high 4EBP1 abundance were resistant (Fig. 4, A and B). Next, we sought to determine whether high 4EBP1 protein abundance primed cells for resistances to MLN0128. To this end, we knocked down 4EBP1 using pooled small interfering RNA (siRNAs) to amounts comparable to those observed in the "low 4EBP1" clones (Fig. 4C). Remarkably, knockdown of 4EBP1 in resistant cells increased their sensitivity to MLN0128 (Fig. 4D). Moreover, enforced expression of wild-type 4EBP1 conferred resistance to a previously sensitive clone exhibiting low 4EBP1 abundance (fig. S7, D and E). At a molecular level, decreasing 4EBP1 mRNA and protein to amounts equivalent to those in sensitive cells appeared to increase de novo protein synthesis (Fig. 4E) and increased the formation of the eIF4E complex (Fig. 4F). Hence, high 4EBP1 abundance directly inhibited the activity of eIF4E by skewing the amount of eIF4G and eIF4A bound to eIF4E, thereby lowering the amount of protein synthesis and conferring resistance to PI3K-AKT-mTOR pathway inhibitors. These findings implicate 4EBP1 as a marker and mediator of drug resistance.

High 4EBP1 abundance is associated with resistance to PI3K inhibitors in prostate cancer patients

Next, we sought to determine whether increased 4EBP1 abundance is a common feature of resistance to inhibitors of the PI3K-AKT-mTOR signaling pathway in prostate cancer patients. To this end, tissues obtained from prostate cancer patients enrolled in an ongoing, phase 2 clinical trial with the oral pan-PI3K inhibitor buparlisib (BKM120) were used to determine total abundance of 4EBP1 before and after PI3K-AKT-mTOR pathway inhibition (www.clinicaltrials.gov; NCT01695473). In this neoadjuvant trial, newly diagnosed prostate cancer patients are treated with 100 mg of buparlisib daily for 14 days before radial prostatectomy (Fig. 5A). Paired diagnostic prostate core biopsy and radical prostatectomy tissue specimens were collected from each patient for pharmacodynamic evaluation. PI3K pathway inhibition was confirmed by phosphorylated AKT immunohistochemistry in nearly all (seven of nine) patients (fig. S8A). The two patients who did not exhibit significant differences had low baseline phosphorylated AKT abundance in the pretreatment setting (fig. S8A). Prostate-specific antigen (PSA) is a biomarker commonly used to monitor treatment response or disease progression. We found that no patients experienced an objective PSA response, defined as a >30% decrease in PSA serum concentration, to BKM120 during the course of the trial (fig. S8B), and this was associated with a significant enrichment of high 4EBP1–expressing luminal epithelial cells (CK8^{+}) posttreatment compared to pretreatment specimens (Fig. 5, B and C). Thus, increased 4EBP1 abundance may characterize a specific epithelial cell type with intrinsic resistance to PI3K-AKT-mTOR pathway inhibition in prostate cancer patients.

DISCUSSION

The PI3K pathway drives tumor growth in prostate cancer, but resistance is often observed to PI3K pathway inhibitors. We found a cell type–specific

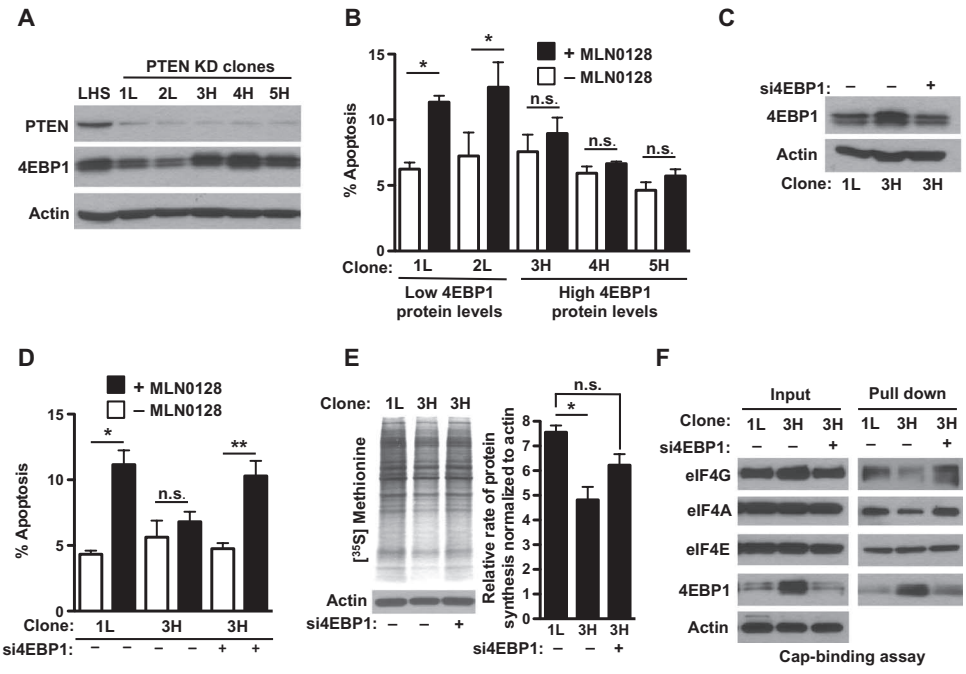

Fig. 4. Increased abundance of 4EBP1 is required to maintain resistance to PI3K pathway inhibitors and is a marker of resistant cells in human prostate cancer. (**A**) Representative Western blot analysis from two experiments for PTEN and 4EBP1 in PTEN KD LHS PrEC clones and control LHS cells. (**B**) Analysis of apoptosis by propidium iodide/annexin V staining in PTEN KD LHS PrECs after 12-hour exposure to MLN0128 or vehicle (–MLN0128) (n = 5 replicates in two independent experiments; $^{*}P < 0.0001$, $^{**}P = 0.04$, t test). (**C**) Representative Western blot of 4EBP1 in PTEN KD LHS PrECs with and without si4EBP1. (**D**) Analysis of apoptosis by propidium iodide/annexin V staining of PTEN KD LHS PrECs after transfection with a 4EBP1-targeted siRNA pool (n = 8 replicates in two independent experiments; $^{*}P < 0.0001$, $^{**}P = 0.005$, t test). (**E**) Representative autoradiograph (left) and quantification of [^{35}S]methionine incorporation assays in PTEN KD LHS PrEC clones upon silencing 4EBP1 [n = 3 independent experiments; $^{*}P < 0.05$, ANOVA (analysis of variance)]. (**F**) Representative cap-binding assay in PTEN KD LHS clones upon silencing 4EBP1. Data are means ± SEM.

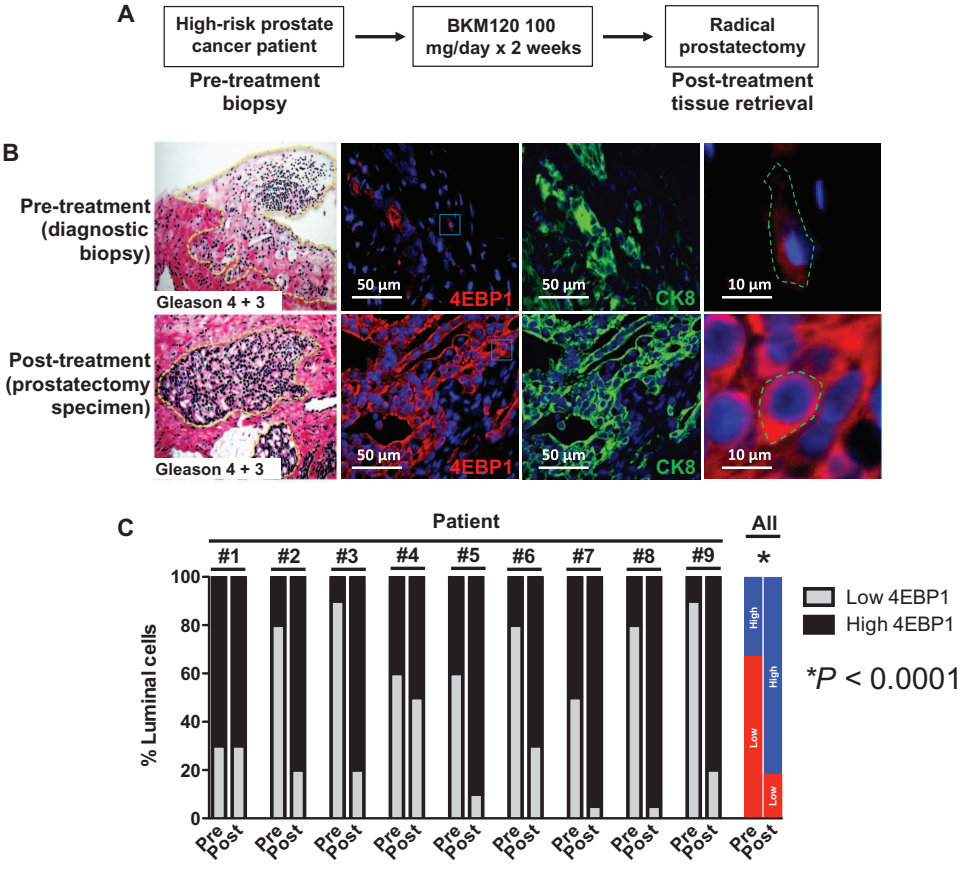

Fig. 5. Increased 4EBP1 abundance is associated with drug resistance in prostate cancer patients. (**A**) Schematic of the phase 2 neoadjuvant BKM120 clinical trial conducted at the University of California, San Francisco (UCSF). (**B**) Representative H&E, CK8, and 4EBP1 immunofluorescence images of a patient tumor before and after treatment with the PI3K inhibitor BKM120. Far right: Magnified insets from the 4EBP1 images. Scale bars, 50 and 10 µm, respectively. (**C**) Quantification of the percentage of luminal epithelial cells with low or high abundance of 4EBP1 for each patient as well as the average for all of the patients before (pre) and after (post) treatment with BKM120 ($^{*}P < 0.0001$, t test).

intrinsic resistance mechanism to PI3K pathway inhibitors in luminal epithelial prostate cells that was mediated by increased abundance of the translation repressor 4EBP1. Compared to luminal cells, basal epithelial cells in the prostate had considerably lower mRNA and protein abundance of 4EBP1, greater protein synthesis activity, and increased MLN0128 sensitivity. Thus, contrary to the expected outcome of increased PI3K signaling resulting in equivalent eIF4E activation across all prostate epithelial cell types, our data uncovered cell type specificity in 4EBP1 transcript abundance that primes cells for drug sensitivity or resistance. In the future, it will be interesting to determine the molecular basis for the increased *4EBP1* expression in luminal epithelial cells compared to basal epithelial cells and whether these differences arise from transcription factor promoter binding (*26*, *27*), chromatin remodeling, or mRNA degradation rates.

The clinical implication of these findings is the in vivo realization of a critical mode of resistance to PI3K pathway inhibitors other than those that have been previously proposed. For example, direct mutations of PI3K pathway components have been described to confer resistance to PI3K-mTOR inhibitors in prostate cancer (*28*), as have parallel mitogenic signaling pathways driven by the androgen receptor (*29*, *30*). In addition to pathway-mediated mechanisms of resistance, the Brugge laboratory has demonstrated that the physical location of a cancer cell within a three-dimensional culture can determine its sensitivity to PI3K pathway inhibitors (*31*). However, unlike these observations, which demonstrate adaptive resistance mechanisms, our findings illustrate the central importance of cell identity dictated by the status of the 4EBP1-eIF4E axis and protein synthesis rates to determine intrinsic resistance to PI3K-AKT-mTOR inhibition. This may be a cellular mechanism akin to oncogene addiction where the genetic makeup of the cell dictates its drug sensitivities (*32*).

Loss of 4EBP1 or increased eIF4E, which is associated with increased protein synthesis, has been previously shown to confer drug-resistant phenotypes in cell culture and xenografts (*33*–*37*). In the context of our in vivo studies, it is therefore intriguing to speculate as to why cancer-prone cells with high 4EBP1 abundance associated with lower protein synthesis rates escape target inhibition. Specific cell types, such as luminal epithelial cells with high 4EBP1 abundance, may harbor more quiescent features associated with lower protein synthesis and therefore may be less sensitive to therapeutic agents that impinge on protein synthesis control coupled to growth and survival. Together, our findings along with previously published reports (*33*–*37*) suggest that there is both a lower and upper threshold of protein synthesis rates that can prime cells for drug resistance. Thus, 4EBP1 abundance, which our study here indicated is cell type–specific (in the prostate) and correlated with mRNA translation, is a distinguishing factor that might be used to predict sensitivity or resistance to PI3K pathway inhibitors in patients.

MATERIALS AND METHODS

Mice

PTEN$^{L/L}$ and Rosa-LSL-rtTA$^{KI/KI}$ mice where obtained from Jackson Laboratories. PB-Cre$^{Tg/+}$ mice were obtained from the Mouse Models of Human Cancers Consortium. All mice were maintained in the C57BL/6 background. The TetO-4EBP1$^{M/M}$ was generated as previously described (*15*). Mice were maintained under specific pathogen–free conditions, and experiments were performed in compliance with institutional guidelines as approved by the Institutional Animal Care and Use Committee of UCSF. Doxycycline (Sigma) was administered in the drinking water at 2 g/liter.

Cell lines and reagents

The LHS PrECs were provided by P. Febbo (UCSF) and were cultured as previously described (*25*). A PTEN-targeted short hairpin RNA (shRNA) sequence 5′-GACTTAGACTTGACCTATATT-3′ (TRCN0000355842, Broad Institute) was cloned into the pLKO.1 vector and overexpressed using standard lentiviral packaging constructs. The PTEN shRNA virus was infected into LHS PrECs. Single-cell clones were selected using trypsin-soaked sterile cloning discs (Sigma). MLN0128 was provided by K. Shokat (UCSF) and used at 1 mg/ml in the preclinical trial and at 100 nM in the cell lines. 4EBP1 siRNAs were obtained from Thermo Scientific (ON-TARGETplus SMARTpool human eIF4EBP1 siRNA, catalog no. L-003005-00). Lipofectamine 2000 (Life Technologies) was used to transfect LHS PrECs with siRNA. The wild-type V5-tagged 4EBP1 construct (pLX304-4EBP1-V5) was provided by P. Paddison (Fred Hutchinson Cancer Research Center).

Clonogenic assay

In brief, 5000 PTEN-deficient LHS cells were plated on to a 35-mm six-well plate. The covering medium was changed every 2 or 3 days during culture. After 14 days, the cells were fixed and stained with crystal violet solution (10% acetic acid, 10% ethanol, and 0.06% crystal) and then visualized. Colonies were enumerated and averaged over three independent experiments.

Prostate tissue processing

Whole mouse prostates were removed from wild-type, 4EBP1^{M}, PTEN$^{L/L}$, and PTEN$^{L/L}$;4EBP1^{M} mice, microdissected, and frozen in liquid nitrogen. Frozen tissues were subsequently manually disassociated using a biopulverizer (BioSpec) and additionally processed for protein and mRNA analysis as described below.

Prostate epithelium single-cell dissociation

Wild-type, 4EBP1^{M}, PTEN$^{L/L}$, and PTEN$^{L/L}$;4EBP1^{M} mouse prostates were retrieved, microdissected, and minced using a scalpel. Tissue chunks were incubated in collagenase I (1 mg/ml; Life Technologies) in Dulbecco's modified Eagle's medium (DMEM), 10% fetal bovine serum (FBS), L-glutamine, and penicillin/streptomycin for 1 to 2 hours at 37°C. This was followed by further dissociation with 0.05% trypsin, which was quenched using fully supplemented DMEM and 500 U of deoxyribonuclease (DNase) (Roche). Cells were manually dissociated with an 18-gauge followed by a 20-gauge needle and syringe. Cells were counted using a hemocytometer.

Western blot analysis

Western blot analysis was performed as previously described (*15*) with antibodies specific to eIF4A (Cell Signaling), eIF4G (Cell Signaling), eIF4E (BD Biosciences), PTEN (Cell Signaling), 4EBP1 (Cell Signaling), phosphorylated 4EBP1 Thr$^{37/46}$ (Cell Signaling), AKT (Cell Signaling), phosphorylated AKT Ser^{473} (Cell Signaling), rpS6 (Cell Signaling), phosphorylated rpS6 Ser$^{240/244}$ (Cell Signaling), PTEN (Cell Signaling), GAPDH (Cell Signaling) and β-actin (Sigma), phosphorylated eEF2 Thr^{56} (Cell Signaling), eEF2 (Cell Signaling), PDCD4 (Cell Signaling), phosphorylated eIF2α Ser^{51} (Cell Signaling), eIF2α (Cell Signaling), and 4EBP2 (Cell Signaling). Densitometry analysis was completed using ImageJ (http://imagej.nih.gov/ij/).

qPCR analysis

RNA was isolated using the manufacturer's protocol for RNA extraction with TRIzol reagent (Invitrogen) using the Pure Link RNA Mini Kit (Invitrogen). RNA was DNase-treated with PureLink DNase (Invitrogen). DNase-treated RNA was transcribed to complementary DNA (cDNA) with SuperScript III First-Strand Synthesis System for Reverse Transcription PCR (Invitrogen), and 1 microliter of cDNA was used to run each SYBR Green detection qPCR assay (SYBR Green Supermix and MyiQ2, Bio-Rad). Primers were used at 200 nM. Oligomer sequences are in table S1.

FACS of distinct prostate epithelial populations

Live prostate epithelial cells were counted and labeled with CD49f–phycoerythrin (PE) (eBioscience), Sca-1–PE-Cy7 (BioLegend), CD31–eFluor 450 (eBioscience), CD45–eFluor 450 (eBioscience), and Ter119–eFluor 450 (eBioscience). Data were acquired using a BD FACSCanto (BD Biosciences) and analyzed with FlowJo (v.9.4.10). To calculate the absolute number of cells per populations, we multiplied the percentage of each cell populations with the total number of cells. To sort the basal and luminal populations, dissociated epithelial cells were stained as above and sorted on a BD FACSAria III (BD Biosciences).

Prostate immunofluorescence and analysis

Prostates were dissected from mice and fixed in 10% formalin overnight at 4°C. Tissues were subsequently dehydrated in ethanol (Sigma) at room temperature, mounted into paraffin blocks, and sectioned at 5 microns per tissue slice. Specimens were deparaffinized and rehydrated using CitriSolv (Fisher) followed by serial ethanol washes. Antigen unmasking was performed on each section using citrate (pH 6; Vector Laboratories) in a pressure cooker at 125°C for 10 to 30 min. Sections were washed in distilled water followed by two washes in tris-buffered saline (TBS). The sections were then incubated in 5% goat serum, 1% bovine serum albumin in TBS for 1 hour at room temperature. Various primary antibodies were used including those specific for cytokeratin 5 (Covance), cytokeratin 8 (Abcam), total 4EBP1 (Cell Signaling), phosphorylated AKT Ser^{473} (Cell Signaling), and phosphorylated 4EBP1 $Thr^{37/46}$ (Cell Signaling), which were diluted in blocking solution and incubated on sections overnight at 4°C. Specimens were then washed in TBS and incubated with the appropriate Alexa 488– and Alexa 594–labeled secondary antibodies (Invitrogen) at 1:500 for 2 hours at room temperature. A final set of washes in TBS was completed at room temperature followed by mounting with HardSet Mounting Medium with 4′,6-diamidino-2-phenylindole (Vector Laboratories). A Zeiss Axio Imager M1 was used to image the sections. Individual prostate epithelial cells and cancer cells were quantified by mean fluorescence intensity using the Zeiss AxioVision (Release 4.8) densitometric tool. To determine the ratio of luminal epithelial cells to basal epithelial cells, 10 to 15 images were taken for each pharmacologic or genetic manipulation and analyzed. Specifically, a mask for $CK5^+$ basal epithelial cells and $CK8^+$ luminal epithelial cells was drawn for each image and an area was calculated, thereby providing an amount of each cell type (ImageJ). To calculate the ratio, luminal epithelial areas were divided by basal epithelial areas and graphed (GraphPad Inc.).

Hematoxylin and eosin staining

Paraffin-embedded prostate specimens were deparaffinized and rehydrated as described above (see immunofluorescence section), stained with hematoxylin (Thermo Scientific), and washed with water. This was followed by a brief incubation in differentiation ready-to-use solution (VWR) and two washes with water, followed by two 70% ethanol washes. The samples were then stained with eosin (Thermo Scientific) and dehydrated with ethanol, followed by CitriSolv (Fisher). Slides were mounted with Cytoseal XYL (Richard-Allan Scientific).

Apoptosis analysis

TUNEL staining of optimal cutting temperature–embedded prostate was conducted per the manufacturer's protocol (Roche). Apoptosis analysis of live prostate epithelial cells was conducted by first labeling single-cell prostate isolates with CD49f-PE (eBioscience), Sca-1–PE-Cy7 (BioLegend), CD31–eFluor 450 (eBioscience), CD45–eFluor 450 (eBioscience), and Ter119–eFluor 450 (eBioscience). This is followed by labeling with annexin V–allophycocyanin (APC) (BD Pharmingen) and 7-AAD (BD Pharmingen) following the manufacturer's instructions (BD Biosciences). Data were acquired using a BD FACSCanto (BD Biosciences) and analyzed with FlowJo (v.9.4.10).

Cell proliferation analysis by BrdU incorporation in vivo

Two hundred microliters of BrdU (10 mg/ml) (BD Pharmingen) was administered by intraperitoneal injection in mice 48 and 24 hours before they were euthanized. Prostates were retrieved and dissociated to single cells as above. Staining for BrdU was conducted using the manufacturer's protocol (BD Pharmingen). In short, cells were labeled with CD49f-PE (eBioscience), Sca-1–PE-Cy7 (BioLegend), CD31–eFluor 450 (eBioscience), CD45–eFluor 450 (eBioscience), and Ter119–eFluor 450 (eBioscience), subsequently fixed, and permeabilized with BD Cytofix/Cytoperm buffer. Cells were treated with DNAse to expose the BrdU epitopes and were stained with APC–anti-BrdU antibody. Data were acquired using a BD FACSCanto (BD Biosciences) and analyzed with FlowJo (v.9.4.10).

Ultrasound imaging of the mouse prostate

A Vevo 770 ultrasound imaging system (VisualSonics) was used to image $PTEN^{L/L}$ and $PTEN^{L/L}$;$4EBP1^{M}$ anterior prostates before and after doxycycline treatment. Areas of interest were measured by assessing the largest area (height and width) of each mass within the anterior prostate.

Ex vivo [^{35}S]methionine labeling in primary prostate epithelial cells

Primary basal and luminal epithelial cells from wild-type and $PTEN^{L/L}$ mice were dissociated and sorted as described above. For each cell type, 40,000 cells were incubated with 33 mCi of [^{35}S]methionine for 1.5 hours in methionine-free DMEM (Invitrogen) plus 10% dialyzed FBS and L-glutamine. Cells were prepared using a standard protein lysate protocol, resolved on a 10% SDS–polyacrylamide gel, and transferred onto a polyvinylidene difluoride membrane (Bio-Rad). The membrane was exposed to autoradiography film (Denville) for 24 hours and developed. Densitometry analysis was completed using ImageJ (http://imagej.nih.gov/ij/). For the LHS PTEN KD PrECs, 250,000 cells were plated and incubated as described above.

Neoadjuvant BKM120 prostate cancer clinical trial

A phase 2 prospective pharmacodynamic study of buparlisib (BKM120) (*38*), an oral pan-class PI3K inhibitor, in patients with high-risk, localized prostate cancer was conducted at UCSF (NCT01695473). The primary study objective was to determine the proportion of men with downstream target inhibition of PI3K in prostate tumor tissue, as measured by immunohistochemistry. Eligible subjects had localized adenocarcinoma of the prostate that were candidates for and had selected radical prostatectomy as the primary treatment. Subjects had high-risk disease, defined as Gleason ≥8 and ≥2 discrete core biopsies containing ≥20% cancer or Gleason 4 + 3 and ≥50% of core biopsies containing cancer. Patients were required to have adequate diagnostic core biopsy specimens for pharmacodynamic evaluation; patients who did not have adequate specimens for evaluation were required to undergo a pretreatment biopsy for tissue acquisition. Patients received buparlisib 100 mg daily for the 14 days preceding radical prostatectomy, with the final dose taken on the night before surgery. The study was conducted in accordance with International Conference on Harmonization good clinical practice standards, with approval by the institutional review board at UCSF. All patients provided written informed consent to participate.

Cap-binding assay

Cells were lysed in buffer A [10 mM tris-HCl (pH 7.6), 140 mM KCl, 4 mM $MgCl_2$, 1 mM dithiothreitol, 1 mM EDTA, and protease inhibitors

supplemented with 1% NP-40], and cell lysates (250 μg of protein in 500 μl) were incubated overnight at 4°C with 50 μl of the mRNA cap analog m^7GTP-Sepharose (Jena Bioscience) in buffer A, under constant and gentle agitation. The protein complex Sepharose beads were washed with buffer A supplemented with 0.5% NP-40, and the eIF4E-associated complex was resolved by SDS–polyacrylamide gel electrophoresis and Western blotting.

SUPPLEMENTARY MATERIALS

www.sciencesignaling.org/cgi/content/full/8/403/ra116/DC1

Fig. S1. Absolute quantification of basal epithelial cells and luminal epithelial cells after treatment with MLN0128.

Fig. S2. qPCR phenotyping of distinct sorted epithelial cell populations in wild-type and $PTEN^{L/L}$ mice.

Fig. S3. Efficiency of *PTEN* deletion and the phosphorylation and localization of 4EBP1 in basal and luminal epithelial cells in vivo.

Fig. S4. Western blot analysis of translation initiation factors and regulators in wild-type and $PTEN^{L/L}$ basal and luminal epithelial cells.

Fig. S5. $4EBP1^{M}$ does not affect normal prostate homeostasis but impedes prostate cancer initiation and progression.

Fig. S6. Effect of PTEN loss and $4EBP1^{M}$ expression on absolute number of basal and luminal epithelial cells.

Fig. S7. Expression of 4EBP1 endows resistance to MLN0128 in LHS PTEN KD cell lines.

Fig. S8. Phosphorylated AKT (Ser^{473}) immunohistochemistry of prostate tumors and serum PSA concentrations from patients before and after treatment with BKM120.

Table S1. qPCR oligonucleotide sequences.

REFERENCES AND NOTES

1. B. S. Taylor, N. Schultz, H. Hieronymus, A. Gopalan, Y. Xiao, B. S. Carver, V. K. Arora, P. Kaushik, E. Cerami, B. Reva, Y. Antipin, N. Mitsiades, T. Landers, I. Dolgalev, J. E. Major, M. Wilson, N. D. Socci, A. E. Lash, A. Heguy, J. A. Eastham, H. I. Scher, V. E. Reuter, P. T. Scardino, C. Sander, C. L. Sawyers, W. L. Gerald, Integrative genomic profiling of human prostate cancer. *Cancer Cell* **18**, 11–22 (2010).
2. N. Choi, B. Zhang, L. Zhang, M. Ittmann, L. Xin, Adult murine prostate basal and luminal cells are self-sustained lineages that can both serve as targets for prostate cancer initiation. *Cancer Cell* **21**, 253–265 (2012).
3. T. Stoyanova, A. R. Cooper, J. M. Drake, X. Liu, A. J. Armstrong, K. J. Pienta, H. Zhang, D. B. Kohn, J. Huang, O. N. Witte, A. S. Goldstein, Prostate cancer originating in basal cells progresses to adenocarcinoma propagated by luminal-like cells. *Proc. Natl. Acad. Sci. U.S.A.* **110**, 20111–20116 (2013).
4. X. Wang, M. Kruithof-deJulio, K. D. Economides, D. Walker, H. Yu, M. V. Halili, Y.-P. Hu, S. M. Price, C. Abate-Shen, M. M. Shen, A luminal epithelial stem cell that is a cell of origin for prostate cancer. *Nature* **461**, 495–500 (2009).
5. A.-C. Gingras, B. Raught, S. P. Gygi, A. Niedzwiecka, M. Miron, S. K. Burley, R. D. Polakiewicz, A. Wyslouch-Cieszynska, R. Aebersold, N. Sonenberg, Hierarchical phosphorylation of the translation inhibitor 4E-BP1. *Genes Dev.* **15**, 2852–2864 (2001).
6. A.-C. Gingras, S. G. Kennedy, M. A. O'Leary, N. Sonenberg, N. Hay, 4E-BP1, A repressor of mRNA translation, is phosphorylated and inactivated by the Akt(PKB) signaling pathway. *Genes Dev.* **12**, 502–513 (1998).
7. A. C. Hsieh, Y. Liu, M. P. Edlind, N. T. Ingolia, M. R. Janes, A. Sher, E. Y. Shi, C. R. Stumpf, C. Christensen, M. J. Bonham, S. Wang, P. Ren, M. Martin, K. Jessen, M. E. Feldman, J. S. Weissman, K. M. Shokat, C. Rommel, D. Ruggero, The translational landscape of mTOR signalling steers cancer initiation and metastasis. *Nature* **485**, 55–61 (2012).
8. D. Ruggero, L. Montanaro, L. Ma, W. Xu, P. Londei, C. Cordon-Cardo, P. P. Pandolfi, The translation factor eIF-4E promotes tumor formation and cooperates with c-Myc in lymphomagenesis. *Nat. Med.* **10**, 484–486 (2004).
9. A. Lazaris-Karatzas, K. S. Montine, N. Sonenberg, Malignant transformation by a eukaryotic initiation factor subunit that binds to mRNA 5′ cap. *Nature* **345**, 544–547 (1990).
10. A. Haghighat, N. Sonenberg, eIF4G dramatically enhances the binding of eIF4E to the mRNA 5′-cap structure. *J. Biol. Chem.* **272**, 21677–21680 (1997).
11. G. W. Rogers Jr., N. J. Richter, W. C. Merrick, Biochemical and kinetic characterization of the RNA helicase activity of eukaryotic initiation factor 4A. *J. Biol. Chem.* **274**, 12236–12244 (1999).
12. A. Pause, G. J. Belsham, A.-C. Gingras, O. Donzé, T.-A. Lin, J. C. Lawrence Jr., N. Sonenberg, Insulin-dependent stimulation of protein synthesis by phosphorylation of a regulator of 5′-cap function. *Nature* **371**, 762–767 (1994).
13. M. P. Edlind, A. C. Hsieh, PI3K-AKT-mTOR signaling in prostate cancer progression and androgen deprivation therapy resistance. *Asian J. Androl.* **16**, 378–386 (2014).
14. S. Wang, J. Gao, Q. Lei, N. Rozengurt, C. Pritchard, J. Jiao, G. V. Thomas, G. Li, P. Roy-Burman, P. S. Nelson, X. Liu, H. Wu, Prostate-specific deletion of the murine Pten tumor suppressor gene leads to metastatic prostate cancer. *Cancer Cell* **4**, 209–221 (2003).
15. A. C. Hsieh, M. Costa, O. Zollo, C. Davis, M. E. Feldman, J. R. Testa, O. Meyuhas, K. M. Shokat, D. Ruggero, Genetic dissection of the oncogenic mTOR pathway reveals druggable addiction to translational control via 4EBP-eIF4E. *Cancer Cell* **17**, 249–261 (2010).
16. D. Lawson, Y. Zong, S. Memarzadeh, L. Xin, J. Huang, O. Witte, Basal epithelial stem cells are efficient targets for prostate cancer initiation. *Proc. Natl. Acad. Sci. U.S.A.* **107**, 2610–2615 (2010).
17. I. Ruvinsky, N. Sharon, T. Lerer, H. Cohen, M. Stolovich-Rain, T. Nir, Y. Dor, P. Zisman, O. Meyuhas, Ribosomal protein S6 phosphorylation is a determinant of cell size and glucose homeostasis. *Genes Dev.* **19**, 2199–2211 (2005).
18. J. R. Graff, B. W. Konicek, R. L. Lynch, C. A. Dumstorf, M. S. Dowless, A. M. McNulty, S. H. Parsons, L. H. Brail, B. M. Colligan, J. W. Koop, B. M. Hurst, J. A. Deddens, B. L. Neubauer, L. F. Stancato, H. W. Carter, L. E. Douglass, J. H. Carter, eIF4E activation is commonly elevated in advanced human prostate cancers and significantly related to reduced patient survival. *Cancer Res.* **69**, 3866–3873 (2009).
19. C. Andrieu, D. Taieb, V. Baylot, S. Ettinger, P. Soubeyran, A. De-Thonel, C. Nelson, C. Garrido, A. So, L. Fazli, F. Bladou, M. Gleave, J. L. Iovanna, P. Rocchi, Heat shock protein 27 confers resistance to androgen ablation and chemotherapy in prostate cancer cells through eIF4E. *Oncogene* **29**, 1883–1896 (2010).
20. S. A. F. Morad, M. Schmid, B. Büchele, H.-U. Siehl, M. El Gafaary, O. Lunov, T. Syrovets, T. Simmet, A novel semisynthetic inhibitor of the FRB domain of mammalian target of rapamycin blocks proliferation and triggers apoptosis in chemoresistant prostate cancer cells. *Mol. Pharmacol.* **83**, 531–541 (2013).
21. X. Wu, J. Wu, J. Huang, W. C. Powell, J. F. Zhang, R. J. Matusik, F. O. Sangiorgi, R. E. Maxson, H. M. Sucov, P. Roy-Burman, Generation of a prostate epithelial cell-specific Cre transgenic mouse model for tissue-specific gene ablation. *Mech. Dev.* **101**, 61–69 (2001).
22. G. Belteki, J. Haigh, N. Kabacs, K. Haigh, K. Sison, F. Costantini, J. Whitsett, S. E. Quaggin, A. Nagy, Conditional and inducible transgene expression in mice through the combinatorial use of Cre-mediated recombination and tetracycline induction. *Nucleic Acids Res.* **33**, e51 (2005).
23. O. Pinter, Z. Beda, Z. Casaba, I. Gerendai, Differences in the onset of puberty in selected inbred mouse strains. *Endocrine Abstracts* **14**, 617 (2007).
24. L. Furic, L. Rong, O. Larsson, I. H. Koumakpayi, K. Yoshida, A. Brueschke, E. Petroulakis, N. Robichaud, M. Pollak, L. A. Gaboury, P. P. Pandolfi, F. Saad, N. Sonenberg, eIF4E Phosphorylation promotes tumorigenesis and is associated with prostate cancer progression. *Proc. Natl. Acad. Sci. U.S.A.* **107**, 14134–14139 (2010).
25. R. Berger, P. G. Febbo, P. K. Majumder, J. J. Zhao, S. Mukherjee, S. Signoretti, K. T. Campbell, W. R. Sellers, T. M. Roberts, M. Loda, T. R. Golub, W. C. Hahn, Androgen-induced differentiation and tumorigenicity of human prostate epithelial cells. *Cancer Res.* **64**, 8867–8875 (2004).
26. R. Azar, A. Alard, C. Susini, C. Bousquet, S. Pyronnet, 4E-BP1 is a target of Smad4 essential for TGFβ-mediated inhibition of cell proliferation. *EMBO J.* **28**, 3514–3522 (2009).
27. R. Azar, C. Lasfargues, C. Bousquet, S. Pyronnet, Contribution of HIF-1α in *4E-BP1* gene expression. *Molec. Cancer Res.* **11**, 54–61 (2013).
28. E. R. Zunder, Z. A. Knight, B. T. Houseman, B. Apsel, K. M. Shokat, Discovery of drug-resistant and drug-sensitizing mutations in the oncogenic PI3K isoform p110α. *Cancer Cell* **14**, 180–192 (2008).
29. B. S. Carver, C. Chapinski, J. Wongvipat, H. Hieronymus, Y. Chen, S. Chandarlapaty, V. K. Arora, C. Le, J. Koutcher, H. Scher, P. T. Scardino, N. Rosen, C. L. Sawyers, Reciprocal feedback regulation of PI3K and androgen receptor signaling in PTEN-deficient prostate cancer. *Cancer Cell* **19**, 575–586 (2011).
30. D. J. Mulholland, L. M. Tran, Y. Li, H. Cai, A. Morim, S. Wang, S. Plaisier, I. P. Garraway, J. Huang, T. G. Graeber, H. Wu, Cell autonomous role of PTEN in regulating castration-resistant prostate cancer growth. *Cancer Cell* **19**, 792–804 (2011).
31. T. Muranen, L. M. Selfors, D. T. Worster, M. P. Iwanicki, L. Song, F. C. Morales, S. Gao, G. B. Mills, J. S. Brugge, Inhibition of PI3K/mTOR leads to adaptive resistance in matrix-attached cancer cells. *Cancer Cell* **21**, 227–239 (2012).
32. I. B. Weinstein, Cancer. Addiction to oncogenes—The Achilles heal of cancer. *Science* **297**, 63–64 (2002).
33. L. Boussemart, H. Malka-Mahieu, I. Girault, D. Allard, O. Hemmingsson, G. Tomasic, M. Thomas, C. Basmadjian, N. Ribeiro, F. Thuaud, C. Mateus, E. Routier, N. Kamsu-Kom, S. Agoussi, A. M. Eggermont, L. Désaubry, C. Robert, S. Vagner, EIF4F is a nexus of resistance to anti-BRAF and anti-MEK cancer therapies. *Nature* **513**, 105–109 (2014).
34. S. Mallya, B. A. Fitch, J. S. Lee, L. So, M. R. Janes, D. A. Fruman, Resistance to mTOR kinase inhibitors in lymphoma cells lacking 4EBP1. *PLOS One* **9**, e88865 (2014).
35. C. L. Cope, R. Gilley, K. Balmanno, M. J. Sale, K. D. Howarth, M. Hampson, P. D. Smith, S. M. Guichard, S. J. Cook, Adaptation to mTOR kinase inhibitors by amplification of eIF4E to maintain cap-dependent translation. *J. Cell Sci.* **127**, 788–800 (2014).

36. T. Alain, M. Morita, B. D. Fonseca, A. Yanagiya, N. Siddiqui, M. Bhat, D. Zammit, V. Marcus, P. Metrakos, L.-A. Voyer, V. Gandin, Y. Liu, I. Topisirovic, N. Sonenberg, eIF4E/4E-BP ratio predicts the efficacy of mTOR targeted therapies. *Cancer Res.* **72**, 6468–6476 (2012).
37. N. Ilic, T. Utermark, H. R. Widlund, T. M. Roberts, PI3K-targeted therapy can be evaded by gene amplification along the MYC-eukaryotic translation initiation factor 4E (eIF4E) axis. *Proc. Natl. Acad. Sci. U.S.A.* **108**, E699–E708 (2011).
38. J. C. Bendell, J. Rodon, H. A. Burris, M. de Jonge, J. Verweij, D. Birle, D. Demanse, S. S. De Buck, Q. C. Ru, M. Peters, M. Goldbrunner, J. Baselga, Phase I, dose-escalation study of BKM120, an oral pan-Class I PI3K inhibitor, in patients with advanced solid tumors. *J. Clin. Oncol.* **30**, 282–290 (2012).

Acknowledgments: We thank M. Barna for critical reading of the manuscript and J. Shen for editing; B. Hann of the UCSF Preclinical Therapeutics Core for technical advice regarding ultrasound imaging; J. Gordon of the UCSF Laboratory for Cell Analysis for technical advice with FACS; M. Meng and M. Cooperberg for enrolling patients onto the BKM120 trial; A. Foye, A. Toschi, and J. Youngren for BKM120 clinical trial tissue acquisition; Goldberg-Benioff Program in Cancer Translational Biology for their support and commitment to prostate cancer research; and L. Wang and Y. Liu for technical support. We also thank P. Paddison (Fred Hutchinson Cancer Research Center) for gifting the pLX304-4EBP1-V5 construct, P. Febbo (UCSF) for the LHS PrECs, and K. Shokat (UCSF) for MLN0128. **Funding:** A.C.H. is supported by a Burroughs Wellcome Fund Career Award for Medical Scientists, by the Prostate Cancer Foundation, and by the NIH (1K08CA175154). A.C.H. is a V Foundation for Cancer Research scholar. D.R. is supported by the NIH (1R01CA154916 and 1R01CA184624) and a Stand Up to Cancer/Prostate Cancer Foundation Prostate Dream Team Translational Cancer Research Grant. This research grant is made possible by the support of the Movember Foundation. Stand Up to Cancer is a program of the Entertainment Industry Foundation administered by the American Association for Cancer Research. D.R. is a Leukemia and Lymphoma Society Research Scholar. **Author contributions:** A.C.H. and D.R. conceived of and designed all experiments. A.C.H., L.W., H.G.N., and M.P.E. conducted all experiments. W.K. was the lead investigator for the BKM120 phase 2 clinical trial. P.R.C. provided prostate cancer specimens through the BKM120 clinical trial. A.C.H. and D.R. analyzed the data and wrote the manuscript. All authors discussed results and edited the manuscript. **Competing interests:** The authors declare that they have no competing interests.

Submitted 23 September 2015
Accepted 30 October 2015
Final Publication 17 November 2015
10.1126/scisignal.aad5111
Citation: A. C. Hsieh, H. G. Nguyen, L. Wen, M. P. Edlind, P. R. Carroll, W. Kim, D. Ruggero, Cell type–specific abundance of 4EBP1 primes prostate cancer sensitivity or resistance to PI3K pathway inhibitors. *Sci. Signal.* **8**, ra116 (2015).

Cell type–specific abundance of 4EBP1 primes prostate cancer sensitivity or resistance to PI3K pathway inhibitors

Andrew C. Hsieh, Hao G. Nguyen, Lexiaochuan Wen, Merritt P. Edlind, Peter R. Carroll, Won Kim and Davide Ruggero (November 17, 2015)

Science Signaling **8** (403), ra116. [doi: 10.1126/scisignal.aad5111]